

1 **Impact of fossil and non-fossil sources on the molecular compositions of water soluble humic-**  
2 **like substance in PM<sub>2.5</sub> at a suburb site of Yangtze River Delta, China**

3  
4 Mengying Bao<sup>1,2,3</sup>, Yan-Lin Zhang<sup>1,2,\*</sup>, Fang Cao<sup>1,2</sup>, Yihang Hong<sup>1,2</sup>, Yu-Chi Lin<sup>1,2</sup>, Mingyuan Yu<sup>1,2</sup>,  
5 Hongxing Jiang<sup>4,5</sup>, Zhineng Cheng<sup>4,5</sup>, [Rongshuang Xu<sup>1,2</sup>](#), Xiaoying Yang<sup>1,2</sup>

6  
7 *1 School of Applied Meteorology, Nanjing University of Information Science & Technology,*  
8 *Nanjing 210044, China.*

9 *2 Atmospheric Environment Center, Joint Laboratory for International Cooperation on Climate*  
10 *and Environmental Change, Ministry of Education (ILCEC), Nanjing University of Information*  
11 *Science & Technology, Nanjing 210044, China.*

12 *3 Huzhou Meteorological Administration, Huzhou 313300, China*

13 *4 State Key Laboratory of Organic Geochemistry and Guangdong province Key Laboratory of*  
14 *Environmental Protection and Resources Utilization, Guangzhou Institute of Geochemistry,*  
15 *Chinese Academy of Sciences, Guangzhou 510640, China.*

16 *5 CAS Center for Excellence in Deep Earth Science, Guangzhou 510640, China*

17 *Correspondence: Yan-Lin Zhang ([dryanlinzhang@outlook.com](mailto:dryanlinzhang@outlook.com))*

18  
19 **Abstract**

20 Atmospheric humic-like substances (HULIS) affect global radiation balance due to ~~their~~  
21 strong light absorption at the ultraviolet wavelength. The potential sources and molecular  
22 compositions of water soluble HULIS at a suburb site of Yangtze River Delta from 2017 to 2018  
23 were discussed based on the radiocarbon (<sup>14</sup>C) analysis combining the Fourier Transform Ion  
24 Cyclotron Resonance Mass Spectrometry (FT-ICR MS) technique in this study. The <sup>14</sup>C results  
25 showed that the averaged non-fossil source contributions to HULIS were 39 ± 8 % and 36 ± 6 %  
26 in summer and winter, respectively, **indicating the significant contributions from fossil sources to**  
27 **HULIS** ~~indicating that both the fossil and non-fossil sources played important roles in the formation~~  
28 ~~of HULIS~~. The Van Krevelen diagrams obtained from the FT-ICR MS results showed that the  
29 proportions of tannins-like and carbohydrates-like groups were higher in summer, suggesting  
30 significant contribution of HULIS from biogenic secondary organic aerosols (SOA). The higher  
31 proportions of condensed aromatic structures in winter suggested ~~the~~ increasing anthropogenic

**Formatted:** Font: (Default) Times New Roman, 12 pt,  
Font color: Auto, Highlight

**Formatted:** Font: (Default) Times New Roman, 12 pt,  
Font color: Auto

32 emissions. Molecular composition analysis on the CHO, CHON, CHOS, and CHONS subgroups  
33 showed the relatively higher intensities of high O-containing macromolecular oligomers in CHO  
34 compounds in summer, further indicating stronger biogenic SOA formation in summer. High-  
35 intensity phenolic substances and flavonoids which were related to biomass burning and polycyclic  
36 aromatic hydrocarbons (PAHs) derivatives indicating fossil fuel combustion emissions were found  
37 in winter CHO compounds. High-intensity phenolic substances and flavonoids which were related  
38 to biomass burning and polycyclic aromatic hydrocarbons (PAHs) derivatives indicating fossil fuel  
39 combustion emissions were found in winter CHO compounds. Besides, two high-intensity CHO  
40 compounds containing condensed aromatic ring structures (C<sub>9</sub>H<sub>6</sub>O<sub>7</sub> and C<sub>10</sub>H<sub>5</sub>O<sub>8</sub>) identified in  
41 summer and winter samples were similar to those from off-road engine samples, indicating that  
42 traffic emission was one of the important fossil sources of HULIS at the study site. The CHON  
43 compounds were mainly composed of ~~organonitrates or~~ nitro compounds ~~or organonitrates~~ -with  
44 significant higher intensities in winter, which was associated to biomass burning emission, as well  
45 as the enhanced formation of organonitrates due to high NO<sub>x</sub> in winter. However, the high-intensity  
46 CHON molecular formulas in summer were referring to N-heterocyclic aromatic compounds,  
47 which were produced from the atmospheric secondary processes involving reduced N species (e.g.,  
48 ammonium). The S-containing compounds were mainly composed of organosulfates (OSs)  
49 derived from biogenic precursors, long-chain alkane and aromatic hydrocarbon, illustrating the  
50 mixed sources of HULIS, further illustrating the mixed sources of HULIS. Generally, different  
51 policies need to be considered for each season due to the different season sources, i.e., biogenic  
52 emission in summer and biomass burning in winter for non-fossil source, and both important  
53 biogenic and anthropogenic source contributions to HULIS at the study site, traffic emission and  
54 anthropogenic SOA formation in both seasons and additional coal combustion in winter. Measures  
55 to control emissions from motor vehicles and industrial processes need to be considered in summer.  
56 Additional control measures on coal power plants and biomass burning should be concerned in  
57 winter. These findings add to our understanding of the interaction between the sources and the  
58 molecular compositions of atmospheric HULIS.

59

## 60 1. Introduction

61 Atmospheric humic-like substances (HULIS) have been observed worldwide and can be  
62 produced from primary combustion of biomass, fossil fuel, as well as various secondary processes

Formatted: Highlight

Formatted: Highlight

Formatted: Highlight

Formatted: Highlight

Formatted: Font: (Default) Times New Roman, (Asian)  
+Body Asian (等线), Font color: Auto, Highlight

Formatted: Highlight

Formatted: Font: (Default) Times New Roman, (Asian)  
+Body Asian (等线), Font color: Auto, Highlight

Formatted: Highlight

Formatted: Highlight

Formatted: Font color: Auto, Highlight

Formatted: Font color: Auto, Highlight

Formatted: Font color: Auto, Highlight

63 such as photochemical processes of volatile organic compounds (VOCs) and heterogeneous  
64 reactions of organic aerosols in the atmosphere (Kuang et al., 2015; Li et al., 2019; Ma et al., 2018;  
65 Sun et al., 2021). As important component of brown carbon (BrC) aerosols, HULIS species have  
66 been widely reported to have a great impact on global radiative budget, contributing to 20-40% of  
67 the direct radiative forcing caused by light absorbing aerosols due to its light absorption at the  
68 ultraviolet wavelength (Chung et al., 2012; Zhang et al., 2017; Zhang et al., 2020<sup>a</sup>; Wang et al.,  
69 ~~2018b~~2018<sup>c</sup>). HULIS are a highly complex mixture of polar organic compounds composed of  
70 aromatic and hydrophobic aliphatic structures containing carboxyl, carbonyl, and hydroxyl  
71 function groups (Zheng et al., 2013; Graber and Rudich, 2006; Zhang et al., 2022<sup>b</sup>; Zhang et al.,  
72 2022<sup>c</sup>). During the atmospheric secondary oxidation processes, the substitutions of hydrophilic  
73 functional groups ~~produced increased~~ aerosol hygroscopicity (Huo et al., 2021; Jiang et al., 2020).  
74 Polycarboxylic acids in HULIS are surface-active and play an important role in the cloud  
75 condensation nuclei (CCN) activity (Tsui and McNeill, 2018). N-base compounds can promote  
76 the generation of atmospheric reactive oxygen species (ROS) which have a great impact on human  
77 health (Wang et al., ~~2017b~~2017<sup>c</sup>; De Haan et al., 2018; Song et al., 2022). Identifying the  
78 molecular compositions of HULIS is a challenge due to complex mixtures contained in HULIS  
79 and can help to a better understanding of the processes involving organic compounds in  
80 atmosphere (Noziere et al., 2015; Laskin et al., 2018).

81 The Fourier-Transform Ion Cyclotron Resonance Mass Spectrometry (FT-ICR MS) coupled  
82 with electrospray ionization (ESI) ion source have been widely used in identifying the chemical  
83 structure of HULIS, providing high mass accuracy and can determine molecular formulas from  
84 mixed compounds (Chen et al., 2016; Wang et al., 2019b; Lin et al., 2012a; Jiang et al., 2020).  
85 Typical molecular formulas composed of C, H, and O atoms in HULIS were observed being  
86 abundant in carboxylic acids, ~~lignin~~lignin-derived products, and polycyclic aromatic hydrocarbons  
87 (PAHs) or their derivatives (Lin et al., 2012a; Sun et al., 2021; Jiang et al., 2020; Huo et al., 2021;  
88 Song et al., 2018). In addition, the HULIS formation of N and S containing precursors ~~was~~also  
89 widely detected. The N-containing compounds such as nitroaromatics were important  
90 chromophores in HULIS in aged biomass burning organic aerosols (BBOA), as well as in ambient  
91 aerosols influenced by biomass burning (BB), while reduced N compounds such as N-heterocyclic  
92 aromatic compounds were found to be important chromophores in fresh BBOA (Wang et al.,  
93 2019b; Song et al., 2022; Jiang et al., 2020; Wang et al., ~~2017b~~2017<sup>c</sup>). Recent laboratory

Formatted: Highlight

Formatted: Highlight

Formatted: Highlight

Formatted: Highlight

Formatted: Highlight

Formatted: Highlight

Formatted: Highlight

94 simulation experiments showed that the photooxidation of various anthropogenic VOCs (e.g.,  
95 naphthalene, benzene, toluene, and ethylbenzene) would be promoted under high NO<sub>x</sub> condition,  
96 producing strongly light absorbing nitroaromatics (Yang et al., 2022; Aiona et al., 2018; Siemens  
97 et al., 2022; Xie et al., 2017). Otherwise, nighttime oxidation of biogenic or anthropogenic VOCs,  
98 such as benzene/toluene, isoprene (C<sub>5</sub>H<sub>8</sub>) and monoterpenes (C<sub>10</sub>H<sub>16</sub>) by NO<sub>3</sub> radicals lead to  
99 substantial organonitrates formation, where the VOCs oxidation is strongly affected by NO<sub>x</sub> (He  
100 et al., 2021; Shen et al., 2021; Wang et al., 2020; Zheng et al., 2021).

101 The organosulfates (OSs) and nitrooxy organosulfates (nitrooxy-OSs) have also been found  
102 to widely exist in HULIS in different atmospheric environment (Lin et al., 2012b; Lin et al., 2012a;  
103 Sun et al., 2021). Field study and laboratory smog chamber experiments have confirmed that OSs  
104 and nitrooxy-OSs in the atmosphere mainly come from the O<sub>3</sub>, OH, or NO<sub>3</sub> oxidation of biogenic  
105 VOCs such as isoprene, α/β-pinene as well as aromatic hydrocarbon in the presence of H<sub>2</sub>SO<sub>4</sub>/SO<sub>2</sub>  
106 (Surratt et al., 2008; Glasius et al., 2021; Yang et al., 2020; Lin et al., 2012b; Huang et al., 2020).  
107 Coal combustions were found to be important sources of the aromatic OSs and nitrooxy-OSs in  
108 HULIS (Song et al., 2018). Besides, the long-chain alkanes were found to be important precursor  
109 of OSs in atmospheric aerosol samples from urban area which was related to vehicle emissions  
110 (Wang et al., 2019a; Tao et al., 2014).

111 Nanjing is one of the main cities in the Yangtze River Delta (YRD), which is one of the most  
112 developed areas in China. Organic matter can account for 20-40% of PM<sub>2.5</sub> in the YRD area due  
113 to the impact of complicated sources, especially anthropogenic emissions (Wang et al., 2017a;  
114 Wang et al., 2016a). Studies have reported that BrC is an important contributor to aerosol light  
115 absorption in Nanjing and exhibited obvious seasonal variations, with peaks in wintertime, owing  
116 to emissions from biomass burning, fossil fuel combustion, and secondary formation (Chen et al.,  
117 2018; Cui et al., 2021; Xie et al., 2020; Wang et al., 2018a). Recently, works on the field  
118 observation of nitrated aromatic compounds (NACs) were conducted to explore the light  
119 absorption contributions of NACs to BrC and help to better understand the links between the  
120 optical properties and molecular compositions of BrC (Gu et al., 2022; Cao et al., 2023). However,  
121 as far as we know, understanding of the sources of atmospheric HULIS at molecular levels was  
122 still limited. In this work, Previous study reported by our laboratory have found significant HULIS  
123 formation at Nanjing, China influenced by both biogenic and anthropogenic emissions (Bao et al.,  
124 2022). The molecular compositions of water soluble HULIS isolated from PM<sub>2.5</sub> samples

- Formatted: Highlight
- Formatted: Highlight
- Formatted: Highlight
- Formatted: Highlight
- Formatted: Highlight
- Formatted: Font: (Default) Times New Roman, 12 pt, Font color: Auto, Highlight
- Formatted: Font: (Default) Times New Roman, 12 pt, Highlight
- Formatted: Font: (Default) Times New Roman, 12 pt, Highlight
- Formatted: Highlight
- Formatted: Highlight
- Formatted: Highlight
- Formatted: Highlight
- Formatted: Highlight
- Formatted: Highlight
- Formatted: Highlight
- Formatted: Highlight

125 collected in summertime and wintertime from 2017 to 2018 at Nanjing, China, were investigated  
126 combining the FT-ICR MS and radiocarbon ( $^{14}\text{C}$ ) analysis. We aim to obtain the molecular  
127 characteristic differences of water soluble HULIS in summertime and wintertime and to get a better  
128 understanding of the influence of different sources on the molecular compositions of HULIS.

## 129 2. Materials and methods

### 130 2.1 Sample collection

131 The 24 h  $\text{PM}_{2.5}$  samples were collected on the roof of Wende building, which was about 21  
132 m height from the ground at Nanjing University of Information Science and Technology (32.2° N,  
133 118.7° E) using a high-volume sampler (KC-1000, Qingdao, China) at a flow rate of 300 L  $\text{min}^{-1}$ .  
134 The study site was located ~~inat~~ the north suburb area of Nanjing, adjacent to G205 State Road and  
135 surrounded by an industrial park and residential area. Generally, the study site was affected by  
136 human activity, industrial emission, and traffic emission. The sample collection was conducted in  
137 summer from 12 August 2017 to 26 August 2017 and in winter from 31 December 2017 to 31  
138 January 2018. A heavy haze event occurred from 31 December 2017 to 3 January 2018, thus the  
139 sample frequency was adjusted to 2 h in daytime and 8 h in nighttime. Field blank filters were  
140 performed before and after sample collection for each season. More details about the sample  
141 collection can be found in previous research ~~reported by Bao et al. (2022). reported by our~~  
142 ~~laboratory (Bao et al., 2022).~~ The air pollutants data including  $\text{PM}_{2.5}$ ,  $\text{SO}_2$  and  $\text{NO}_2$  were provided  
143 by China National Environmental Monitoring Centre. Twelve samples were selected for further  
144 chemical analysis and the details about the sample selection are described in Section 3.1 in this  
145 study.

### 146 2.2 Chemical analysis

147 ~~\_\_\_\_\_~~ The solid phase extraction (SPE) cartridge (Oasis HLB, 30  $\mu\text{m}$ , 60 mg/cartridge, Waters,  
148 USA) was performed to isolate the water soluble HULIS in this study. Briefly, ~~and the prepared~~  
149 water extracts -passed through the pre-conditioned HLB cartridge firstly, then the retained HULIS  
150 on the HLB cartridge were eluted with 2% (v/v) ammonia/methanol and evaporated to dryness  
151 under a gentle stream of nitrogen gas, then re-dissolved in ultrapure water for the measurement.  
152 The carbon fraction in HULIS (HULIS-C) were determined using a total carbon analyzer  
153 (Shimadzu-TOC-VCPH, Shimadzu, Japan) with standard deviation of reproducibility test less than  
154 3.5% and detection limit of 0.14  $\mu\text{g C m}^{-3}$ . More details about the HULIS isolation and  
155 measurement have been described in (Bao et al., (2022).

Formatted: Highlight

Formatted: Highlight

156  
157 The mass concentrations of levoglucosan, water soluble ions including  $\text{NO}_3^-$ ,  $\text{NH}_4^+$  and  $\text{SO}_4^{2-}$   
158 were measured using an ion chromatography (Dionex ICS-5000+, ThermoFisher Scientific, USA)  
159 separated on an AS11 column (4\*250 mm, Dionex). Potassium hydrate (KOH) was used as the  
160 gradient eluent for anion determination. The levoglucosan concentrations were analyzed using the  
161 same ion chromatograph equipped with a CarboPac MA1 analytical column (4\*250 mm, Dionex)  
162 and an electrochemical detector. Sodium hydroxide (NaOH) was used as the gradient eluent for  
163 levoglucosan determination. All data were blank corrected in this study. ~~and More~~ the details of  
164 the methods have been described previously (Liu et al., 2019). ~~All data were blank corrected in~~  
165 ~~this study. More details about the HULIS isolation and measurement have been described in (Bao~~  
166 ~~et al., 2022).~~

Formatted: Highlight

Formatted: Highlight

Formatted: Highlight

Formatted: Highlight

Formatted: Font color: Black

### 167 2.3 Radiocarbon analysis

168 For the radiocarbon measurement of the HULIS samples, the organic solvents were firstly  
169 evaporated under a gentle flow of ultrapure  $\text{N}_2$  for 30-40 minutes in tin cups. After that, the tin  
170 cups were wrapped into balls and more than 50  $\mu\text{g}$  of carbon from the HULIS samples was  
171 combusted into  $\text{CO}_2$  using an elemental analyzer (EA, model vario micro, elemental, Germany),  
172 then reduced into graphite targets for  $^{14}\text{C}$  determination at the State Key Laboratory of Organic  
173 Geochemistry, Guangzhou Institute of Geochemistry, Guangzhou, China (Jiang et al., 2020).  
174 Detailed descriptions of the  $^{14}\text{C}$  data processing can be found in previous study (Mo et al., 2018).  
175 Briefly, the  $^{14}\text{C}$  values were expressed as the modern carbon ( $f_m$ ) fraction after correcting for the  
176  $\delta^{13}\text{C}$  fractionation. The  $f_m$  was converted into non-fossil carbon ( $f_{\text{nf}}$ ) fraction with the correction  
177 factor of  $1.06 \pm 0.07$  based on the long-term time series of  $^{14}\text{CO}_2$  sampled at the background station  
178 in this study (Levin et al., 2013; Levin and Kromer, 2004).  $^{14}\text{C}$  analysis of the oxalic acid standard  
179 (IAEA-C7) was conducted in this study (Xu et al., 2021). No field blank correction was performed  
180 for the carbon isotope analysis since the carbon content in the field blanks was negligible.

Formatted: Highlight

Formatted: Font: (Default) Times New Roman, 12 pt,  
Font color: Auto, Highlight

Formatted: Highlight

Formatted: Font: (Default) Times New Roman, 12 pt,  
Font color: Auto, Highlight

Formatted: Font: (Default) Times New Roman, 12 pt,  
Font color: Auto, Highlight

Formatted: Font: (Default) Times New Roman, 12 pt,  
Font color: Auto

### 181 2.4 High-resolution FT-ICR MS analysis

182 The ultrahigh resolution mass spectra of the HULIS samples were obtained through a Solarix  
183 XR FT-ICR MS (Bruker Daltonics, GmbH, Bremen, Germany) equipped with a 9.4 T  
184 superconducting magnet (Gamry Instruments, Warminster, USA) and a Paracell analyzer cell  
185 (Brucker Daltonik GmbH, Bremen, Germany) in the negative ESI mode. The detection mass range  
186 was set as  $m/z$  150 to 800 and the ion accumulation time was set as 0.65 s. A total of 100 continuous

187 4M transient data points were superposed to enhance the signal to noise ratio and dynamic range.  
188 The mass spectrum was externally calibrated with a standard solution of arginine and internal  
189 recalibration was performed using typical O<sub>6</sub>S<sub>1</sub> chemical species in DataAnalysis ver. 4.4 software  
190 (Bruker Daltonics) (Mo et al., 2018; Tang et al., 2020; Jiang et al., 2020). Field blank filters were  
191 analyzed as same as the samples and all the sample data were blank corrected. More details about  
192 the data processing can be found in Text S1 in the supporting information.

### 193 3. Results and discussion

#### 194 3.1 General temporal characteristics during the sampling periods

195 Figure 1 displays the temporal variations of non-fossil contributions to HULIS-C, the mass  
196 concentrations of HULIS-C, levoglucosan, NO<sub>3</sub><sup>-</sup>, SO<sub>4</sub><sup>2-</sup>, NH<sub>4</sub><sup>+</sup>, SO<sub>2</sub>, NO<sub>2</sub>, and PM<sub>2.5</sub>, as well as the  
197 relative humidity and temperature during the study periods corresponding to the 12 samples. **The**  
198 **12 samples were named as S1-S6 (summer) and W1-W6 (winter), in chronological order**  
199 **corresponding to the six samples in summer and winter, respectively** in this study. The averaged  
200 mass concentrations of PM<sub>2.5</sub> in summer and winter during the selected periods were 21.05 ± 8.05  
201 μg m<sup>-3</sup> and 445.67 ± 275.00 μg m<sup>-3</sup>, respectively, indicating the serious pollution level in winter.  
202 The daily PM<sub>2.5</sub> mass concentrations in summer were all below the daily averaged Chinese  
203 National Ambient Air Quality Standard **(NAAQS) of 35 μg m<sup>-3</sup> for the first grade**, while the daily  
204 PM<sub>2.5</sub> mass concentrations in winter all exceeded the daily averaged **NAAQS of 35 μg m<sup>-3</sup> for the**  
205 **first grade**, of which the PM<sub>2.5</sub> mass concentrations of W1-W3 and W6 exceeded 200 μg m<sup>-3</sup>.

206 ~~As shown in Fig. 1, the mass concentrations of HULIS-C, levoglucosan, water soluble~~  
207 ~~secondary inorganic aerosols (SIA), and air pollutants showed similar trends in winter, suggesting~~  
208 ~~the influence of BB and anthropogenic emissions in winter (Wu et al., 2019b).~~ **The averaged mass**  
209 **concentrations of HULIS in summer and winter during the selected periods were 1.83 ± 0.27 μg**  
210 **m<sup>-3</sup> and 4.52 ± 2.29 μg m<sup>-3</sup>, respectively. The averaged HULIS concentration in summer was**  
211 **comparable with those measured in other cities in China, i.e., 1.70 μg m<sup>-3</sup> in Guangzhou, 1.61 μg**  
212 **m<sup>-3</sup> in Shanghai and 1.50 μg m<sup>-3</sup> in Xi'an. Compared with those measured in winter samples in**  
213 **other cities, our result was comparable with those in Xi'an (4.50 μg m<sup>-3</sup>), a little lower than those**  
214 **in the megacity of Shanghai (5.31 μg m<sup>-3</sup>) and higher than those in the southern coastal city of**  
215 **Guangzhou (3.6 μg m<sup>-3</sup>) (Fan et al., 2016; Zhang et al., 2020b; Zhao et al., 2016).**

216 ~~As shown in Fig. 1, the mass concentrations of HULIS-C, levoglucosan, water soluble~~  
217 ~~secondary inorganic aerosols (SIA), and air pollutants showed similar trends in winter, suggesting~~

Formatted: Highlight

Formatted: Highlight

Formatted: Highlight

Formatted: Highlight

Formatted: Highlight

Formatted: Highlight

Formatted: Highlight

Formatted: Highlight

Formatted: Highlight

Formatted: Highlight

Formatted: Highlight

Formatted: Highlight

Formatted: Highlight

Formatted: Highlight



218 the influence of BB and anthropogenic emissions in winter (Wu et al., 2019b). The radiocarbon  
219 analysis results showed that the  $f_{\text{nf}}$  of HULIS-C ranged from 30 % to 50 % with an average  
220 contribution of  $39 \pm 8$  % in summer and ranged from 32 % to 48 % with an average contribution  
221 of  $36 \pm 6$  % in winter, indicating the significant contributions from fossil sources to HULIS at the  
222 study site. Significant increasing of the levoglucosan and HULIS-C mass concentrations were  
223 found from 31 December 2017 to 1 January 2018, corresponding to the W1-W3 samples,  
224 indicating the BB impact during the periods. The maximum of the levoglucosan and HULIS-C  
225 mass concentrations were  $552.79 \mu\text{g m}^{-3}$  and  $7.40 \mu\text{g m}^{-3}$ , respectively. Despite the higher  
226 levoglucosan mass concentrations in the W1-W3 samples, the radiocarbon analysis results showed  
227 that the  $f_{\text{nf}}$  of HULIS-C ranged from 30 % to 50 % with an average contribution of  $39 \pm 8$  % in  
228 summer and ranged from 32 % to 48 % with an average contribution of  $36 \pm 6$  % in winter,  
229 indicating that both fossil and non-fossil sources played important roles in the formation of HULIS  
230 at the study site. There were other emission sources of HULIS in winter other than BB. [Figure  
231 S1 shows the 48 h back trajectories (Fig. S1) showed that of each sample during the selected  
232 periods. [The study site was affected by by the clean air masses from the ocean in summer and the  
233 polluted air masses mainly from the northern heating cities in winter, suggesting the coal  
234 combustion contributions to HULIS in winter (Ma et al., 2018; Sun et al., 2021). In addition,  
235 significant increasing of the levoglucosan and HULIS-C mass concentrations were found from 31  
236 December 2017 to 1 January 2018, corresponding to the W1-W3 samples and the maximum of the  
237 levoglucosan and HULIS-C mass concentrations were  $552.79 \text{ ng m}^{-3}$  and  $7.40 \mu\text{g m}^{-3}$ , respectively,  
238 indicating the BB impact during the periods. -In summer, the study site was affected by both  
239 regional transport from the nearby cities in the north and west of Nanjing and the Donghai Sea.  
240 The anthropogenic emissions from the neighboring cities might cause the anthropogenic SOA  
241 formation, i.e., secondary N-containing and S-containing compounds with aromatic structures  
242 during the atmospheric transport processes, which was discussed in detail in section 3.4 in this  
243 study.

Formatted: Highlight

Formatted: Highlight

Formatted: Highlight

Formatted: Highlight

Formatted: Highlight

Formatted: Highlight

Formatted: Highlight

### 244 3.2 Mass spectra and molecular formula assignments

245 Figure S2 and S3 shows the negative ion ESI FT-ICR mass spectra of HULIS in summer and  
246 winter, respectively. The molecular formulas listed are some of the top ten molecular formulas.  
247 Thousands of peaks are present in the spectra in the range from  $m/z$  150 to  $m/z$  600 and the most  
248 intense ion peaks are those in the range  $m/z$  200-400 in summer and  $m/z$  150-350 in winter. Our



249 results are similar to those found for the ultrahigh resolution mass spectra of water-soluble organic  
250 compounds in particles produced from BB, coal combustion, vehicle exhaust emissions, as well as  
251 in ambient aerosols and cloud water samples, **within a reasonable range** -(Tang et al., 2020; Sun et  
252 al., 2021; Song et al., 2018; Song et al., 2019; Bianco et al., 2018). In this study, the assigned  
253 molecular formulas were classified into the following four main subgroups based on their  
254 elemental compositions: CHO (compounds containing only C, H, and O), CHON (compounds  
255 containing C, H, O and N), CHOS (compounds containing C, H, O, and S), and CHONS  
256 (compounds containing C, H, O, N, and S). As shown in Fig. 2, the proportions of the four  
257 subgroups accounted for the overall formulas followed as CHO (20 %-27 %), CHON (28 %-43 %),  
258 CHOS (19 %-26 %), and CHONS (16 %-26 %) in summer, respectively and CHO (15 %-19 %),  
259 CHON (30 %-40 %), CHOS (21 %-32 %), and CHONS (20 %-29 %) in winter, respectively. The  
260 average proportions of the CHO, CHON, CHOS, and CHONS compounds in summer were  $22 \pm$   
261  $3 \%$ ,  $36 \pm 5 \%$ ,  $22 \pm 3 \%$ , and  $20 \pm 4 \%$ , respectively. The average proportions of the four subgroups  
262 in winter were  $17 \pm 2 \%$ ,  $32 \pm 4 \%$ ,  $24 \pm 3 \%$ , and  $27 \pm 4 \%$ , respectively. **The CHON groups were**  
263 **the major components of molecular formulas, furthermore, the relative intensity of CHON groups**  
264 **increased significantly in winter (Fig. S2 and Fig. S3). Studies have suggested that HULIS emitted**  
265 **from biomass burning can produce a high abundance of CHON compounds and S-containing**  
266 **compounds were the dominant component for primary HULIS emitted from coal combustion**  
267 **(Zhang et al., 2021; Song et al., 2018). The higher intensity of CHON compounds in winter in this**  
268 **study further indicated the BB contribution. Notably, the**The contributions of S-containing  
269 **compounds (CHOS and CHONS groups) increased in winter which might be related to the polluted**  
270 **air masses transported from the northern heating cities with increasing coal combustions emissions**  
271 **in winter (Song et al., 2018). Notably, the relatively higher proportions of CHO and CHON groups**  
272 **in summer were most probably related to the increasing biogenic emissions in summer, resulting**  
273 **in the formation of some high molecular weight oligomers or highly oxidized organonitrates,**  
274 **which was discussed in detail in section 3.4.1 and 3.4.2 in this study.**

275 Table S1 and S2 displays the composition characteristics of atmospheric HULIS in the  
276 summer and winter samples, including the relative intensity weighted average values of number,  
277 molecular weight ( $MW_w$ ), elemental ratios ( $O/C_w$  and  $H/C_w$ ), double-bond equivalent ( $DBE_w$ ),  
278 aromaticity index ( $AI_w$ ), and  $DBE/C_w$ . A total of 14387 and 15731 peaks were detected in the  
279 summer and winter samples, respectively. The O/C and H/C ratios are commonly calculated to

Formatted: Highlight

Formatted: Highlight

Formatted: Highlight

Formatted: Highlight

Formatted: Highlight

Formatted: Highlight

Formatted: Font color: Auto, Highlight

Formatted: Highlight

Formatted: Highlight

Formatted: Font color: Auto, Highlight

Formatted: Highlight

Formatted: Font color: Auto, Highlight

280 evaluate the oxidation degree and saturation degree of the compounds, respectively (Ning et al.,  
281 2022). The  $O/C_w$  values were in a range of 0.61-0.80 with an average value of  $0.71 \pm 0.07$  for  
282 summer samples and in a range of 0.59-0.67 with an average value of  $0.62 \pm 0.03$  for winter  
283 samples, respectively. The higher oxidation degree of summer samples than winter samples  
284 indicated stronger secondary HULIS formation in summer. The  $H/C_w$  values were in a range of  
285 1.38-1.46 with an average value of  $1.42 \pm 0.03$  for summer samples and in a range of 1.33-1.41  
286 with an average value of  $1.36 \pm 0.04$  for winter samples, respectively. The  $O/C_w$  and  $H/C_w$  of each  
287 molecular subgroup followed a changing trend of  $CHO < CHON < CHOS < CHONS$  compounds.  
288 Most of the S-containing compounds had a  $O/C$  value  $\geq 0.7$ , suggesting the large amounts of highly  
289 oxidized OSs in S-containing compounds which contained various functional groups and were  
290 mainly from the photochemical oxidation of biogenic or anthropogenic volatile organic  
291 compounds (VOCs) (Mutzel et al., 2015). The DBE values were calculated to describe the degree  
292 of unsaturation of compounds and restricted the assigned molecular formulas with unreasonably  
293 high or low number of rings or double bonds (Kroll et al., 2011). The related parameter DBE/C  
294 was the double-bond equivalent of unit carbon which can reflect the condensed ring structures in  
295 the compounds (Jiang et al., 2021). The higher DBE<sub>w</sub> and DBE/C<sub>w</sub> values of CHO and CHON  
296 compounds were found in this study, indicating the higher unsaturation degree of these two groups.

Formatted: Highlight

Formatted: Highlight

Formatted: Highlight

297 Considering that double bonds can be formed by heteroatoms especially O atoms, whereas  
298 make no contributions to the aromaticity of the compounds,  $AI_w$  was calculated to supplement the  
299 DBE results (Song et al., 2018; Ning et al., 2019).  $AI_w$  can eliminate the contribution of O, N, and  
300 S atoms to the C=C double bond density of molecules. The  $AI_w$  values of different compounds  
301 groups in HULIS presented the changing trends:  $AI_w(CHONS) > AI_w(CHON) > AI_w(CHO) >$   
302  $AI_w(CHOS)$  in summer and  $AI_w(CHON) > AI_w(CHO) > AI_w(CHONS) > AI_w(CHOS)$  in winter,  
303 respectively. The formulas can be classified into three parts based on AI values proposed by  
304 previous studies: aliphatic ( $AI=0$ ), olefinic ( $0 < AI \leq 0.5$ ) and aromatic ( $AI > 0.5$ ) (Koch and Dittmar,  
305 2006). As shown in Fig. S4 and S5, the aliphatic were the main components of S-containing  
306 compounds in this study and the olefinic and aromatic were the main components of CHO and  
307 CHON compounds. Furthermore, the aromatic proportion of CHO and CHON compounds  
308 significantly increased in winter, suggesting the increasing anthropogenic emissions in winter.

309 3.3 Comparative analysis using Van Krevelen diagrams

310 In this study, the Van Krevelen diagrams (Fig. 3) were constructed to display the molecular  
311 composition and categorical distribution of the collected samples (Noziere et al., 2015; Patriarca  
312 et al., 2018; Li et al., 2022). According to the elemental ratios (O/C and H/C ratios) and AI values,  
313 seven major compound classes were classified, including lipids-like species, lignins-like species,  
314 proteins-like species, tannins-like species, carbohydrates-like species, condensed aromatics  
315 structure, and unsaturated hydrocarbons (Table S3). The Van Krevelen diagrams showed similar  
316 distributions in the 12 samples. The CHO and CHON compounds located in the lower left area  
317 and the S-containing compounds located in the upper light area with higher O/C and H/C ratios,  
318 indicating a higher degree of oxidation and saturation. The condensed aromatic structure mainly  
319 consisted in CHO and CHON compounds, further suggesting the influence of anthropogenic  
320 emissions on the formation of CHO and CHON compounds.

321 Figure 4 presents the averaged relative contributions of the number of molecular formulas  
322 from the seven categories in summer and winter samples, respectively. Lignins-like species  
323 accounted for the highest proportion of CHO compounds with average contributions of 58 % and  
324 61 % in summer and winter, respectively, followed by CHON compounds with average  
325 contributions of 48 % and 57 % in summer and winter, respectively. Lignins are mainly composed  
326 of carboxyl groups, alicyclic rings, aromatic rings, and other O-containing groups. Previous studies  
327 have reported that lignin was a complex phenolic polymer which usually came from direct  
328 biological emissions or combustions of biofuel (Ning et al., 2019; Boreddy et al., 2021; Sun et al.,  
329 2021). Lignins pyrolysis products and other lignins derived molecules have been shown to be  
330 oxidized into light absorbing BrC chromophore under certain conditions (Fleming et al., 2020).

331 Tannins-like species accounted for 21 %, 27 %, 23 %, and 30 % of CHO, CHON, CHOS, and  
332 CHONS compounds, respectively in summer which were higher than those in winter with  
333 contributions of 13 %, 16 %, 16 %, and 23 % to CHO, CHON, CHOS, and CHONS compounds,  
334 respectively. Tannins-like species are a series of polyphenolic compounds containing hydroxyls  
335 and carboxylic groups which have been widely reported in fogs, cloud water and aerosol samples,  
336 attributing to highly oxidized organic compounds such as OSs or nitrooxy-OSs produced from the  
337 nighttime chemistry between the biogenic VOCs with the NO<sub>3</sub> (Altieri et al., 2009; Bianco et al.,  
338 2018; Ning et al., 2019; Altieri et al., 2008; Shen et al., 2021). Carbohydrates-like species which  
339 contain monosaccharide, alditols, and anhydrosugars mainly consisted in CHONS compounds  
340 which also had a relative higher proportion of 33 % in summer than that of 29 % in winter (Sun et

341 al., 2021).  $C_{10}H_{16}NO_{7-9}S$ , as monoterpene nitrooxy-OSs, showing high relative intensities, were  
342 typical carbohydrates-like species detected in this study which represented biogenic secondary  
343 organic aerosols (SOA) (Ning et al., 2019; Surratt et al., 2008; Wang et al., 2020). Both the higher  
344 proportions of tannins-like and carbohydrates-like classes in summer indicated stronger biogenic  
345 SOA formation in this study.

346 Proteins-like classes mainly consisted in CHOS compounds with average proportions of 29 %  
347 and 38 % in summer and winter, respectively. Proteins contain peptide-like structures formed by  
348 dehydration with different kinds of amino acids and consist of short chains of amino acid residues  
349 (Bianco et al., 2018). These compounds are associated with photochemical oxidation processing  
350 in aerosols, thus resulting in the significant formation of OSs from biogenic or anthropogenic  
351 precursors in this study (Bigg and Leck, 2008).

352 Higher condensed aromatics were detected in winter with average proportions of 14 % in  
353 CHO compounds and 8 % in CHON compounds, respectively which were 2-2.5 times of those in  
354 summer. Condensed aromatics are important components of PAHs which were usually emitted  
355 from incomplete combustion of fossil fuels (Ma et al., 2020). The increase of the proportion of  
356 condensed aromatics in winter indicated the stronger influence of anthropogenic sources on  
357 HULIS formation. The unsaturated hydrocarbons and lipids-like species showed the lowest  
358 molecular number percentage of less than 1 % in this study. Previous studies have shown that the  
359 lipids-like species were the main components of water insoluble organic compounds in aerosols  
360 and could be attributed to monocarboxylic acids (Ning et al., 2022; Wozniak et al., 2008).

361 In summary, both the summer and winter samples were mainly composed of compounds from  
362 biogenic origins (lignins-like, tannins-like, proteins-like, and carbohydrates-like species). More  
363 tannins-like and carbohydrates-like species were detected in summer including large amounts of  
364 highly oxidized OSs or nitrooxy-OSs, indicating biogenic SOA formation. More condensed  
365 aromatic structures in CHO and CHON compounds were detected in winter, owing to increasing  
366 anthropogenic emissions. It is noted that ESI ionization technology is more sensitive for the  
367 identification of polar compounds. Therefore, the low polar or nonpolar compounds, such as PAHs  
368 or their derivatives from fossil sources, were probably underestimated in this study (Jiang et al.,  
369 2014; Lin et al., 2018).

### 370 3.4 Molecular composition of HULIS

#### 371 3.4.1 Molecular characteristics of CHO compounds

Formatted: Highlight

Formatted: Highlight

Formatted: Highlight

372 The O/C<sub>w</sub> and H/C<sub>w</sub> ratios for the CHO compounds were 0.45-0.56 and 1.15-1.30 for the  
373 summer samples and 0.42-0.48 and 0.90-1.02 for the winter samples (Table S1 and S2). The  
374 summer samples showed higher oxidation degree and saturation degree. We firstly plotted the Van  
375 Krevelen diagrams of the four molecular subgroups showing relative intensities for all the 12  
376 samples and similar distributions of the high-intensity compounds were found in the 6 summer  
377 samples and the 6 winter samples, respectively. Then we combined all the data in summer and  
378 winter, respectively. As shown in Fig. 5a and 5d, the CHO compounds in summer with high  
379 relative abundance were located at the area within  $0.2 \leq O/C \leq 1.0$  and  $1.0 \leq H/C \leq 1.7$ , mainly  
380 including lignins-like species and tannins-like species which were closely related to biogenic  
381 emissions. On the contrary, the condensed aromatics showed high relative abundance in winter,  
382 suggesting ~~the~~ obviously different sources of HULIS in summer and winter. The DBE values  
383 increased with the increasing of the C numbers (Fig. 5b and 5e). The high-intensity CHO  
384 compounds in HULIS had DBE values between 3-7 with C numbers from 10 to 20 for summer  
385 samples. In winter, the high-intensity CHO compounds had DBE values between 7-11 with C  
386 numbers from 5 to 15. As mentioned above, the aromatic (AI > 0.5) proportion of CHO compounds  
387 significantly increased in winter, the higher DBE values in winter further indicated the consists of  
388 more highly unsaturated aromatic compounds which reflected the anthropogenic emissions.

389 The CHO compounds were classified according to the number of oxygen atoms to evaluate  
390 the oxygen content. As shown in Fig. 5c and 5f, the high-intensity CHO compounds with 6-11  
391 oxygen atom were detected in summer, such as C<sub>15</sub>H<sub>24</sub>O<sub>6</sub>, C<sub>15</sub>H<sub>22</sub>O<sub>10</sub>, C<sub>18</sub>H<sub>26</sub>O<sub>8</sub>, and C<sub>18</sub>H<sub>26</sub>O<sub>9</sub>,  
392 these highly oxygenated organic molecules with high molecular weight have also been detected in  
393 laboratory  $\alpha$ -pinene ozonolysis SOA (Pospisilova et al., 2020). We further classified the CHO  
394 compounds by different carbon atom numbers. As shown in Fig. S6, the C<sub>17</sub>-C<sub>22</sub> compounds were  
395 the main components of the CHO compounds, accounting for more than 50 % of the total number  
396 of CHO molecular formulas in both summer and winter seasons. However, the total relative  
397 intensities of the CHO compounds in summer were significantly higher than those in winter, of  
398 which the C<sub>23</sub>-C<sub>26</sub> and C<sub>27</sub>-C<sub>32</sub> compounds were enriched in summer. These high molecular weight  
399 compounds were probably oligomers formed from various biogenic precursors, such as isoprene,  
400 sesquiterpene, and monoterpene (Daellenbach et al., 2019; Berndt et al., 2018). The high intensities  
401 of these compounds in summer further indicated the stronger biogenic SOA formation in summer  
402 compared with that in winter.

403 High-intensity CHO compounds with 4-9 oxygen atom were detected in winter (Fig. 5c) of  
404 which the  $C_{14}H_{10}O_4$  formula with a DBE value of 10 appeared the highest intensity, which was  
405 probable functional PAHs and have been reported in HULIS from coal combustion smoke particles  
406 (Song et al., 2019). As shown in Fig. S2 and S3, the  $C_{14}H_{10}O_4$  formula appeared high intensity in  
407 all the winter samples, providing the evidence of coal combustion emissions in winter. Some other  
408 high-intensity compounds in winter, such as  $C_{14}H_8O_4$  and  $C_{14}H_8O_5$  both with DBE values of 11,  
409 and  $C_{13}H_8O_2$ ,  $C_{13}H_8O_5$ , and  $C_{13}H_8O_6$  with DBE values of 10, might refer to hydroxyl substitutions  
410 derived from anthracenedione and xanthone, respectively, which have been reported in secondary  
411 wood combustion products (Bruns et al., 2015).  $C_{15}H_{10}O_6$ ,  $C_{15}H_8O_6$ , and  $C_{16}H_{12}O_7$  which had  
412 DBE values of 11, 12, and 11, respectively, might be flavonoids which had flavone backbone, the  
413 key structure of plant pigments, widely existing in plants in nature and could be important sources  
414 of BrC chromophores in aged BBOA (Fleming et al., 2020; Lin et al., 2016; Huang et al., 2021).  
415 Phenolic substances derived from phenol, guaiacol, and syringol are also widely existed in BBOA,  
416 usually from the pyrolysis of lignins in wood, which also play an important role in aqueous-phase  
417 SOA formation (Boreddy et al., 2021). For instance,  $C_{13}H_{10}O_3$  and  $C_{13}H_{10}O_5$  are guaiacol  
418 derivatives,  $C_{15}H_{16}O_8$  are syringol derivatives and  $C_{18}H_{14}O_6$  and  $C_{18}H_{14}O_7$  are phenol derivatives  
419 (Sun et al., 2021). As shown in Fig. S7, the relative intensities of the CHO compounds mentioned  
420 above produced from BB were found to have similar trends with the mass concentrations of  
421 levoglucosan, which were significantly higher in W1-W3 samples, corresponding to the BB period  
422 from 31 December 2017 to 1 January 2018, providing the evidence of BB influence on HULIS  
423 formation in winter.

424 It is noted that the top compounds  $C_9H_6O_7$  and  $C_{10}H_6O_8$  were detected both in the summer  
425 and winter samples (Fig. S2 and S3), which had DBE values of 7 and 8, respectively, containing  
426 abundant condensed aromatic ring structures with high O numbers. Their peaks were also detected  
427 in the HFO (heavy-fuel-oil)-fueled off-road engine samples reported before, suggesting the traffic  
428 emission contributions to HULIS (Cui et al., 2019). This supported the radiocarbon analysis results  
429 in this study and gave further information that the traffic emissions were important fossil sources  
430 in both summer and winter seasons, which was also found in previous research which reported the  
431 sources of HULIS based on the positive matrix factorization (PMF) model by Bao et al. (2022).;

432 3.4.2 Molecular characteristics of CHON compounds

Formatted: Highlight

Formatted: Highlight

Formatted: Highlight

Formatted: Highlight

Formatted: Highlight

433 The O/C<sub>w</sub> of CHON compounds in summer and winter were 0.57-0.71 and 0.52-0.56,  
434 respectively, while the H/C<sub>w</sub> were 1.20-1.32 and 1.00-1.11, respectively (Table S1 and S2).  
435 Compared with the summer CHON compounds, the winter CHON compounds presented  
436 significantly higher ion abundance (Fig. 6a and 6d). The most abundant CHON subgroups had  
437 DBE values of 4-7 and 3-10 in summer and winter, respectively (Fig. 6b and 6e). Similar with [the](#)  
438 CHO compounds, the higher DBE values of high-intensity CHON compounds in HULIS in winter  
439 indicated a high prevalence of double bonds or ring structures. According to the N and O number,  
440 the CHON compounds were classified into N<sub>1</sub>O<sub>x</sub> (N<sub>1</sub>O<sub>1</sub>-N<sub>1</sub>O<sub>15</sub>) and N<sub>2</sub>O<sub>x</sub> (N<sub>2</sub>O<sub>2</sub>-N<sub>2</sub>O<sub>14</sub>) subgroups  
441 in summer and N<sub>1</sub>O<sub>x</sub> (N<sub>1</sub>O<sub>1</sub>-N<sub>1</sub>O<sub>12</sub>) and N<sub>2</sub>O<sub>x</sub> (N<sub>2</sub>O<sub>2</sub>-N<sub>2</sub>O<sub>12</sub>) subgroups in winter, respectively (Fig.  
442 6c and 6f). NO<sub>8-12</sub> and NO<sub>6-9</sub> compounds were most [ly](#) enriched subgroups in summer and winter,  
443 respectively. More oxygen-enriched CHON compounds containing O number above 9 were  
444 detected in summer, implying the higher oxidation degree for summer samples. In addition, the  
445 N<sub>1</sub>O<sub>x</sub> were both the major compounds represented average of 64 ± 4 % and 61 ± 6 % of the CHON  
446 molecular formulas in summer and winter, respectively, indicating the presence of more single  
447 nitro/amino substituents in CHON compounds in this study.

448 Among the CHON compounds, 95 ± 1 % and 86 ± 3 % CHON compounds had O/N values  
449 ≥3 in summer and winter, respectively in this study, indicating these compounds contained large  
450 amounts of oxidized nitrogen functional groups such as nitro compounds (-NO<sub>2</sub>) and/or  
451 organonitrates (-ONO<sub>2</sub>) and excess oxygen atoms indicated the existence of other oxygen-  
452 containing functional groups (Laskin et al., 2009). The organonitrates formation from NO<sub>3</sub>  
453 oxidation of biogenic or anthropogenic VOCs can affect the interactions between anthropogenic  
454 and natural emissions (He et al., 2021; Shen et al., 2021; Wang et al., 2020). Organonitrates were  
455 found to be important species contributing to SOA formation in [the](#) polluted urban environment,  
456 which were enhanced under high NO<sub>x</sub> level (Zheng et al., 2021). The significant higher relative  
457 intensities of CHON compounds in winter indicated that the high NO<sub>x</sub> environment in winter  
458 promoted the formation of organonitrates and highlighted the importance of organonitrates for SOA  
459 control in polluted environment.

460 Furthermore, we found that the increase of the relative abundance of CHON compounds in  
461 winter was particularly significant in W1-W3 samples (Fig. S2 and S3), corresponding to the BB  
462 episode. Phenols produced from the pyrolysis of lignins can react with NO<sub>3</sub> radicals in the  
463 atmosphere, producing nitrophenols, which have been shown to be important BrC chromophore



464 in BBOA (Wang et al., 2017b,2017c; Lin et al., 2016; Cai et al., 2020). It was reported that the gas-  
465 phase reactions of NO<sub>3</sub> radicals with phenolic substances took place at least 4 orders of magnitude  
466 faster than those with aromatic hydrocarbon and even faster in the aqueous phase (Lin et al., 2017).  
467 Among the top CHON compounds with high relative abundance in W1-W3 samples, such as  
468 C<sub>6</sub>H<sub>4</sub>N<sub>2</sub>O<sub>6</sub> and C<sub>7</sub>H<sub>6</sub>N<sub>2</sub>O<sub>6</sub> both with a DBE values of 5 and 6, respectively, were refer to  
469 nitrophenols containing one or two nitrogen-containing functional groups, which have been widely  
470 reported in aged BBOA, indicating the increasing of the CHON compounds relative intensity in  
471 W1-W3 samples were closely related to BB (Lin et al., 2017; Cai et al., 2020; Mohr et al., 2013;  
472 Kourtchev et al., 2016; Lin et al., 2016). Some other top CHON compounds in winter samples  
473 such as C<sub>9</sub>H<sub>4</sub>NO<sub>4</sub> and C<sub>10</sub>H<sub>6</sub>NO<sub>4</sub> with low O/C and H/C ratios most likely indicated the presence  
474 of condensed aromatic structures in the compounds. The C<sub>9</sub>H<sub>4</sub>NO<sub>4</sub> compounds were most likely  
475 emitted from vehicle emissions which have previously been reported (Cui et al., 2019).

476 It is worth noting that some high-intensity CHON compounds with low O/C and H/C ratios  
477 were detected in summer samples in this study (Fig. 6a), which were closely related to aromatic  
478 compounds from anthropogenic emissions. The top compounds with molecular formulas of  
479 C<sub>8</sub>H<sub>5</sub>N<sub>2</sub>O<sub>2</sub> and C<sub>19</sub>H<sub>11</sub>N<sub>2</sub>O<sub>4</sub>, which had O/N of 2-1 and +2, respectively, both were reduced N  
480 compounds referring to N-heterocyclic compounds. Previously studies have found that the N-  
481 heterocyclic aromatic compounds can be formed through the aldehyde-ammonia reactions (De  
482 Haan et al., 2018; Zhang et al., 2022a). This indicated the important role of reduced N species (e.g.,  
483 ammonium) in the formation of anthropogenic SOA in summer. Our results were consistent with  
484 previous study conducted in Xi'an, China which also found formation of reduced N compounds in  
485 light-absorbing aerosols through ammonia involved reactions in summer (Zeng et al., 2021).

#### 3.4.3 Molecular characteristics of S-containing compounds (CHOS and CHONS compounds)

486 The O/C<sub>w</sub> of CHOS compounds in summer and winter were 0.60-0.79 and 0.56-0.67,  
487 respectively, while the H/C<sub>w</sub> were 1.50-1.54 and 1.53-1.72, respectively. The O/C<sub>w</sub> of CHONS  
488 compounds in summer and winter were 0.82-1.01 and 0.76-0.94, respectively, while the H/C<sub>w</sub>  
489 were 1.57-1.65 and 1.58-1.66, respectively (Table S1 and S2). As shown in Fig. 7a, 7d, 8a, and 8d,  
490 the high-intensity S-containing compounds in summer and winter were both located at the area  
491 where O/C >0.5 and H/C >1.5, respectively. In addition, the relative intensity of S-containing  
492 compounds increased with the O/C ratios, suggesting the S-containing compounds were highly  
493 oxidized. A small number of high-intensity S-containing compounds with O/C <1.0 and H/C <1.0  
494

Formatted: Highlight

Formatted: Highlight

Formatted: Highlight

Formatted: Highlight

Formatted: Highlight

Formatted: Highlight

Formatted: Highlight

Formatted: Highlight

495 were also found in winter in this study, which might be related to OSs and nitrooxy-OSs produced  
496 from the oxidation of aromatic hydrocarbon. The CHOS compounds presenting high relative  
497 abundance were rich in O<sub>6-9</sub>S and O<sub>5-7</sub>S groups in summer and winter, respectively, of which the  
498 DBE values were all below 4. The CHONS compounds were rich in O<sub>8-10</sub>S and O<sub>7-9</sub>S groups in  
499 summer and winter, respectively, of which the DBE values were all below 6 (Fig. 7b, 7e, 7c, 7f,  
500 8b, 8e, 8c, and 8f). Compared with those of the CHO and CHON compounds, the DBE values of  
501 S-containing compounds were significantly lower.

502 Among the S-containing compounds, more than 95 % of the CHOS, CHON<sub>1</sub>S, and CHON<sub>2</sub>S  
503 formulas had O/S ratios greater than 4, 7, and 10, respectively, implying these compounds may  
504 contain organic sulfate functional groups (-OSO<sub>3</sub>) or one or two organic nitrate groups (-ONO<sub>2</sub>)  
505 and these compounds ~~are~~ were more likely OSs or nitrooxy-OSs, presenting lower DBE values  
506 and higher O/C and H/C ratios (Table S5 and S6) (O'Brien et al., 2014). The high-intensity CHONS  
507 compounds observed in this study, such as C<sub>10</sub>H<sub>16</sub>NO<sub>7-9</sub>S, C<sub>10</sub>H<sub>18</sub>NO<sub>8-9</sub>S, C<sub>10</sub>H<sub>18</sub>N<sub>2</sub>O<sub>11</sub>S, and  
508 C<sub>9</sub>H<sub>14</sub>NO<sub>8-9</sub>S could be nitrooxy-OSs derived from **monoterpenes such as limonene and  $\alpha$ -**  
509 **terpinene, and monoterpene** of which we found the formulas in summer contained more oxygen  
510 **atoms, indicating the higher oxidation degree of these nitrooxy-OSs in summer** (Figure S2 and S3)  
511 (Sun et al., 2021; Bruggemann et al., 2020; Wang et al., 2020; Wang et al., ~~2018~~2018).

512 The CHOS compounds with high intensity abundance, such as typical isoprene epoxydiols  
513 (IEPOX) derived OSs with molecular formulas of C<sub>5</sub>H<sub>8</sub>O<sub>7</sub>S and C<sub>5</sub>H<sub>10</sub>O<sub>7</sub>S were both detected in  
514 the summer and winter samples, of which the relative intensity of C<sub>5</sub>H<sub>8</sub>O<sub>7</sub>S were over 80 % in S1,  
515 S2, S5, and S6 samples, indicating the significant isoprene SOA formation in summer (Kourtchev  
516 et al., 2016; Kourtchev et al., 2013). **The results were consistent with the previous research on the**  
517 **sources of HULIS based on positive matrix factorization (PMF) model results reported by our**  
518 **laboratory (Bao et al., (2022)).** The monoterpenes derived OSs such as C<sub>8</sub>H<sub>14</sub>O<sub>6</sub>S, C<sub>8</sub>H<sub>14</sub>O<sub>8</sub>S,  
519 C<sub>10</sub>H<sub>18</sub>O<sub>8</sub>, C<sub>10</sub>H<sub>14</sub>O<sub>6</sub>, and C<sub>11</sub>H<sub>16</sub>O<sub>7</sub> were detected in both summer and winter samples in this study,  
520 which could refer to monoterpene-OSs derived from  $\alpha$ -pinene,  $\alpha$ -terpinene, and limonene (Wang  
521 et al., 2020). Moreover, OSs with high carbon numbers (C  $\geq$  14) such as C<sub>14</sub>H<sub>22</sub>O<sub>7</sub>S, C<sub>14</sub>H<sub>22</sub>O<sub>8</sub>S,  
522 C<sub>14</sub>H<sub>24</sub>O<sub>7</sub>S, C<sub>15</sub>H<sub>26</sub>O<sub>7</sub>S, C<sub>15</sub>H<sub>24</sub>O<sub>7</sub>S, C<sub>15</sub>H<sub>24</sub>O<sub>8</sub>S, and C<sub>16</sub>H<sub>28</sub>O<sub>7</sub>S were also observed in both  
523 summer and winter samples. Long-chain alkanes emitted from vehicle emissions might be  
524 precursors of these OSs which was consistent with the molecular structures of OSs collected in  
525 urban areas affected by traffic emissions such as Shanghai, Los Angeles, and Beijing (Wang et al.,

Formatted: Highlight

Formatted: Highlight

Formatted: Highlight

Formatted: Font: (Default) Times New Roman, (Asian) +Body Asian (等线), Font color: Auto, Highlight

Formatted: Highlight

Formatted: Highlight

Formatted: Highlight

2019a; Tao et al., 2014; Wang et al., 2016). The aromatic OSs such as naphthalene derived OSs with molecular formulas of  $C_{10}H_{10}O_6S$ ,  $C_{10}H_{10}O_7S$ , and  $C_{10}H_{12}O_7S$ , 2-methylnaphthalene derived OSs with molecular formulas of  $C_9H_{12}O_6S$ ,  $C_{11}H_{12}O_7S$ , and  $C_{11}H_{14}O_7S$ , and hydroxybenzene derived OSs with molecular formulas of  $C_6H_6O_5S$  were also observed in this study (Qi et al., 2021; Riva et al., 2015; Blair et al., 2017). Figure S8 further displays the ternary plot of the relative intensities of OSs from biogenic precursors (e.g., isoprene and monoterpenes), long-chain alkanes and aromatic hydrocarbon. As shown in Fig. S8, the biogenic OSs and long-chain alkanes OSs formation were comparable in summer and winter, demonstrating both biogenic and anthropogenic emission contributions to HULIS. The aromatic OSs presented higher relative intensities in winter, further indicating the increasing anthropogenic emissions in winter. The presence of long-chain alkanes derived OSs in both summer and winter seasons provided another evidence that the traffic emission was one of the important fossil sources of HULIS in this study.

Formatted: Highlight

### 3.5 Comparison with organic compounds in source and atmospheric aerosol samples

The O/C and H/C ratios of water soluble HULIS in this study were compared with those of water soluble organic compounds reported in source samples from BB, coal combustions, and vehicle emissions (Tang et al., 2020; Song et al., 2018; Cui et al., 2019; Song et al., 2019), cloud water samples (Bianco et al., 2018; Zhao et al., 2013), rainwater samples (Altieri et al., 2009), fog samples (Brege et al., 2018), as well as aerosol samples collected in Beijing (Jang et al., 2020; Wu et al., 2019a; Wang et al., 2018a), Tianjin (Han et al., 2022), Baoding (Sun et al., 2021), Shanghai (Wang et al., 2017a, 2017b), Guangzhou (Jiang et al., 2021), respectively in China, Mainz (Wang et al., 2018a, 2018b), Cork city (Kourtchev et al., 2014), and Bologna (Brege et al., 2018), respectively in Europe, and Bakersfield (O'Brien et al., 2014) and Virginia (Willoughby et al., 2014), respectively in the United States (Fig. 9). The O/C ratios were obviously higher than those detected in primary BB, coal combustion, and vehicle emission samples. The H/C ratios of the CHO and CHON compounds were comparable with the source samples, indicating the organics in HULIS experienced atmospheric secondary process and the mixed sources of HULIS in this study. The H/C ratios of the S-containing compounds were much higher than those of source samples which could be attributed to the significant organosulfates formation in the atmosphere.

Formatted: Highlight

Formatted: Highlight

The O/C ratios reported in this study were also higher than those reported in aerosol samples in urban area in China, further indicating the serious secondary pollution at Nanjing, China. Among the CHO and CHON compounds, we found that the highest H/C ratio values were observed

557 in the southern city of Guangzhou, followed by those in Nanjing and Shanghai, and the lowest  
558 values were observed in the northern cities such as Beijing, Tianjin, and Baoding, indicating the  
559 higher unsaturation degree of the aerosol samples collected from the northern heating-cities, which  
560 were also considered as the heavy industrial region in China. The higher H/C ratios of aerosol  
561 samples collected in Europe and the United States indicated the less anthropogenic emissions such  
562 as industrial emissions from those areas.

#### 563 4. Conclusions

564 This study focuses on the sources and molecular characteristics differences of water soluble  
565 HULIS in summertime and wintertime from 2017 to 2018 at a suburb site of the YRD, China based  
566 on the radiocarbon analysis and FT-ICR MS measurement with ESI ion source in negative mode.

567 The carbon isotope analysis results highlight both the important fossil and non-fossil source  
568 contributions to HULIS at the study site. A total of 14387 and 15731 peaks were detected in the  
569 summer and winter samples, respectively based on the FT-ICR MS results. The assigned molecular  
570 formulas were classified into CHO, CHON, CHOS, and CHONS subgroups according to their  
571 elemental compositions. The Van Krevelen diagrams showed that more tannins-like and  
572 carbohydrates-like species were detected in summer indicating biogenic SOA formation. Whereas  
573 more compounds containing condensed aromatic structures were detected in winter which were  
574 derived from anthropogenic emissions. The total relative intensity of CHO compounds in summer  
575 were significantly higher than those in winter, containing lots of macromolecular oligomers  
576 derived from biogenic precursors. The high-intensity CHO compounds in winter were mainly  
577 aromatic compounds such as phenolic substances and flavonoids which were related to aged  
578 BBOA and oxidized PAHs most probably from fossil fuel combustion. On the contrary, the total  
579 relative intensity of CHON compounds significantly increased in winter, mainly composed of nitro  
580 compounds or organonitrates. The enhanced formation of nitrophenols in winter indicated the BB  
581 influence. The increasing organonitrates formation in winter highlighted the secondary N-  
582 containing compounds formation via NO<sub>3</sub> radical-initiated oxidation processes. It is worth noting  
583 that the top CHON compounds in summer were referring to aromatic reduced N compounds  
584 produced from the aldehyde-ammonia reactions. The S-containing compounds were mainly  
585 composed of highly oxidized OSs. The monoterpenes derived OSs and long-chain alkanes derived  
586 OSs were widely observed in both summer and winter samples, while the aromatic OSs formation  
587 were found to be more significant in winter. The presence of long-chain alkanes derived OSs

Formatted: Highlight

588 supported the radiocarbon results, ~~proving-indicating~~ that the traffic emission was the important  
589 fossil sources at the study site. ~~The presence of aromatic secondary N-containing and S-containing~~  
590 ~~compounds provided evidence for the substantial contributions from anthropogenic SOA~~  
591 ~~formation to fossil sources at the study site. These results further verified the work reported before~~  
592 ~~by Bao et al. (2022) based on the PMF model which have found the significant anthropogenic~~  
593 ~~SOA and fossil fuel combustion contributions to HULIS in urban area in China at molecular level.~~  
594 ~~In addition, strong biogenic emission in summer and BB in winter were found in this study. Our~~  
595 ~~results highlighting the equal importance of different control policies for each season in the~~  
596 ~~future. future reduction in both fossil and non-fossil emissions on atmospheric pollution control.~~

Formatted: Highlight

Formatted: Font color: Auto

Formatted: Highlight

Formatted: Highlight

Formatted: Highlight

Formatted: Highlight

Formatted: Highlight

## 598 Acknowledgments

599 This research was financially supported by the National Natural Science Foundation of China  
600 (grant no. 42192512) and the National Natural Science Foundation of China (grant no. 41977305).

## 603 References

- 604
- 605 Aiona, P. K., Luek, J. L., Timko, S. A., Powers, L. C., Gonsior, M., and Nizkorodov, S. A.: Effect  
606 of photolysis on absorption and fluorescence spectra of light-absorbing secondary organic aerosols,  
607 *Acs Earth Space Chem.*, 2, 235-245, 10.1021/acsearthspacechem.7b00153, 2018.
- 608 Altieri, K. E., Seitzinger, S. P., Carlton, A. G., Turpin, B. J., Klein, G. C., and Marshall, A. G.:  
609 Oligomers formed through in-cloud methylglyoxal reactions: Chemical composition, properties,  
610 and mechanisms investigated by ultra-high resolution FT-ICR mass spectrometry, *Atmos.*  
611 *Environ.*, 42, 1476-1490, 10.1016/j.atmosenv.2007.11.015, 2008.
- 612 Altieri, K. E., Turpin, B. J., and Seitzinger, S. P.: Oligomers, organosulfates, and nitrooxy  
613 organosulfates in rainwater identified by ultra-high resolution electrospray ionization FT-ICR  
614 mass spectrometry, *Atmos. Chem. Phys.*, 9, 2533–2542, www.atmos-chem-phys.net/9/2533/2009/  
615 2009.
- 616 Bao, M., Zhang, Y. L., Cao, F., Lin, Y. C., Hong, Y., Fan, M., Zhang, Y., Yang, X., and Xie, F.:  
617 Light absorption and source apportionment of water soluble humic-like substances (HULIS) in  
618 PM<sub>2.5</sub> at Nanjing, China, *Environ. Res.*, 206, 112554, 10.1016/j.envres.2021.112554, 2022.

619 Berndt, T., Mender, B., Scholz, W., Fischer, L., Herrmann, H., Kulmala, M., and Hansel, A.:  
620 Accretion product formation from ozonolysis and OH radical reaction of alpha-Pinene:  
621 mechanistic insight and the influence of isoprene and ethylene, *Environ. Sci. Technol.*, 52, 11069-  
622 11077, 10.1021/acs.est.8b02210, 2018.

623 Bianco, A., Deguillaume, L., Vaitilingom, M., Nicol, E., Baray, J. L., Chaumerliac, N., and  
624 Bridoux, M.: Molecular characterization of cloud water samples collected at the Puy de Dome  
625 (France) by Fourier transform ion cyclotron resonance mass spectrometry, *Environ. Sci. Technol.*,  
626 52, 10275-10285, 10.1021/acs.est.8b01964, 2018.

627 Bigg, E. K., and Leck, C.: The composition of fragments of bubbles bursting at the ocean surface,  
628 *J. Geophys. Res.*, 113, 10.1029/2007jd009078, 2008.

629 Blair, S. L., MacMillan, A. C., Drozd, G. T., Goldstein, A. H., Chu, R. K., Pasa-Tolic, L., Shaw,  
630 J. B., Tolic, N., Lin, P., Laskin, J., Laskin, A., and Nizkorodov, S. A.: Molecular characterization  
631 of organosulfur compounds in biodiesel and diesel fuel secondary organic aerosol, *Environ. Sci.*  
632 *Technol.*, 51, 119-127, 10.1021/acs.est.6b03304, 2017.

633 Boreddy, S. K. R., Hegde, P., Aswini, A. R., and Aryasree, S.: Chemical characteristics, size  
634 distributions, molecular composition, and brown carbon in South Asian outflow to the Indian  
635 Ocean, *Earth. Space. Sci.*, 8, 10.1029/2020ea001615, 2021.

636 Brege, M., Paglione, M., Gilardoni, S., Decesari, S., Facchini, M. C., and Mazzoleni, L. R.:  
637 Molecular insights on aging and aqueous-phase processing from ambient biomass burning  
638 emissions-influenced Po Valley fog and aerosol, *Atmos. Chem. Phys.*, 18, 13197-13214,  
639 10.5194/acp-18-13197-2018, 2018.

640 Bruggemann, M., Xu, R., Tilgner, A., Kwong, K. C., Mutzel, A., Poon, H. Y., Otto, T., Schaefer,  
641 T., Poulain, L., Chan, M. N., and Herrmann, H.: Organosulfates in ambient aerosol: state of  
642 knowledge and future research directions on formation, abundance, fate, and importance, *Environ.*  
643 *Sci. Technol.*, 54, 3767-3782, 10.1021/acs.est.9b06751, 2020.

644 Bruns, E. A., Krapf, M., Orasche, J., Huang, Y., Zimmermann, R., Drinovec, L., Močnik, G., El-  
645 Haddad, I., Slowik, J. G., Dommen, J., Baltensperger, U., and Prévôt, A. S. H.: Characterization  
646 of primary and secondary wood combustion products generated under different burner loads,  
647 *Atmos. Chem. Phys.*, 15, 2825-2841, 10.5194/acp-15-2825-2015, 2015.

648 Cai, J., Zeng, X., Zhi, G., Gligorovski, S., Sheng, G., Yu, Z., Wang, X., and Peng, P. a.: Molecular  
649 composition and photochemical evolution of water-soluble organic carbon (WSOC) extracted

650 from field biomass burning aerosols using high-resolution mass spectrometry, *Atmos. Chem.*  
651 *Phys.*, 20, 6115-6128, 10.5194/acp-20-6115-2020, 2020.

652 [Cao, M., Yu, W., Chen, M., and Chen, M.: Characterization of nitrated aromatic compounds in](#)  
653 [fine particles from Nanjing, China: Optical properties, source allocation, and secondary processes,](#)  
654 [Environ. Pollut.](#), 316, 120650, 10.1016/j.envpol.2022.120650, 2023.

Formatted: Highlight

655 Chen, Q., Ikemori, F., Higo, H., Asakawa, D., and Mochida, M.: Chemical structural  
656 characteristics of HULIS and other fractionated organic matter in urban aerosols: results from mass  
657 spectral and FT-IR analysis, *Environ. Sci. Technol.*, 50, 1721-1730, 10.1021/acs.est.5b05277,  
658 2016.

659 [Chen, Y., Ge, X., Chen, H., Xie, X., Chen, Y., Wang, J., Ye, Z., Bao, M., Zhang, Y., and Chen,](#)  
660 [M.: Seasonal light absorption properties of water-soluble brown carbon in atmospheric fine](#)  
661 [particles in Nanjing, China, Atmos. Environ.](#), 187, 230-240, 10.1016/j.atmosenv.2018.06.002,  
662 2018.

Formatted: Highlight

663 Chung, C. E., Ramanathan, V., and Decremier, D.: Observationally constrained estimates of  
664 carbonaceous aerosol radiative forcing, *Proc. Natl. Acad. Sci. U. S. A.*, 109, 11624-11629,  
665 10.1073/pnas.1203707109, 2012.

666 [Cui, F., Pei, S., Chen, M., Ma, Y., and Pan, Q.: Absorption enhancement of black carbon and the](#)  
667 [contribution of brown carbon to light absorption in the summer of Nanjing, China, Atmos. Pollut.](#)  
668 [Res.](#), 12, 480-487, 10.1016/j.apr.2020.12.008, 2021.

Formatted: Highlight

669 Cui, M., Li, C., Chen, Y., Zhang, F., Li, J., Jiang, B., Mo, Y., Li, J., Yan, C., Zheng, M., Xie, Z.,  
670 Zhang, G., and Zheng, J.: Molecular characterization of polar organic aerosol constituents in off-  
671 road engine emissions using Fourier transform ion cyclotron resonance mass spectrometry (FT-  
672 ICR MS): implications for source apportionment, *Atmos. Chem. Phys.*, 19, 13945-13956,  
673 10.5194/acp-19-13945-2019, 2019.

674 Daellenbach, K. R., Kourtchev, I., Vogel, A. L., Bruns, E. A., Jiang, J., Petäjä, T., Jaffrezo, J.-L.,  
675 Aksoyoglu, S., Kalberer, M., Baltensperger, U., El Haddad, I., and Prévôt, A. S. H.: Impact of  
676 anthropogenic and biogenic sources on the seasonal variation in the molecular composition of  
677 urban organic aerosols: a field and laboratory study using ultra-high-resolution mass spectrometry,  
678 *Atmos. Chem. Phys.*, 19, 5973-5991, 10.5194/acp-19-5973-2019, 2019.

679 De Haan, D. O., Tapavicza, E., Riva, M., Cui, T., Surratt, J. D., Smith, A. C., Jordan, M. C.,  
680 Nilakantan, S., Almodovar, M., Stewart, T. N., de Loera, A., De Haan, A. C., Cazaunau, M.,



681 Gratien, A., Pangu, E., and Doussin, J. F.: Nitrogen-containing, light-Absorbing oligomers  
682 produced in aerosol particles exposed to methylglyoxal, photolysis, and cloud cycling, Environ.  
683 Sci. Technol., 52, 4061-4071, 10.1021/acs.est.7b06105, 2018.

684 [Fan, X., Song, J., and Peng, P. a.: Temporal variations of the abundance and optical properties of  
685 water soluble Humic-Like Substances \(HULIS\) in PM<sub>2.5</sub> at Guangzhou, China, Atmos. Res., 172-  
686 173, 8-15, 10.1016/j.atmosres.2015.12.024, 2016](#)

687 Fleming, L. T., Lin, P., Roberts, J. M., Selimovic, V., Yokelson, R., Laskin, J., Laskin, A., and  
688 Nizkorodov, S. A.: Molecular composition and photochemical lifetimes of brown carbon  
689 chromophores in biomass burning organic aerosol, Atmos. Chem. Phys., 20, 1105-1129,  
690 10.5194/acp-20-1105-2020, 2020.

691 [Gu, C., Cui, S., Ge, X., Wang, Z., Chen, M., Qian, Z., Liu, Z., Wang, X., and Zhang, Y.: Chemical  
692 composition, sources and optical properties of nitrated aromatic compounds in fine particulate  
693 matter during winter foggy days in Nanjing, China, Environ. Res., 212, 113255,  
694 10.1016/j.envres.2022.113255, 2022](#)

695 Glasius, M., Thomsen, D., Wang, K., Iversen, L. S., Duan, J., and Huang, R. J.: Chemical  
696 characteristics and sources of organosulfates, organosulfonates, and carboxylic acids in aerosols  
697 in urban Xi'an, Northwest China, Sci. Total. Environ., 151187, 10.1016/j.scitotenv.2021.151187,  
698 2021.

699 Graber, E. R., and Rudich, Y.: Atmospheric HULIS: How humic-like are they? A comprehensive  
700 and critical review, Atmos. Chem. Phys., 6, 729-753, 10.5194/acp-6-729-2006, 2006.

701 Han, H., Feng, Y., Chen, J., Xie, Q., Chen, S., Sheng, M., Zhong, S., Wei, W., Su, S., and Fu, P.:  
702 Acidification impacts on the molecular composition of dissolved organic matter revealed by FT-  
703 ICR MS, Sci. Total. Environ., 805, 150284, 10.1016/j.scitotenv.2021.150284, 2022.

704 He, Q., Tomaz, S., Li, C., Zhu, M., Meidan, D., Riva, M., Laskin, A., Brown, S. S., George, C.,  
705 Wang, X., and Rudich, Y.: Optical properties of secondary organic aerosol produced by nitrate  
706 radical oxidation of biogenic volatile organic compounds, Environ. Sci. Technol., 55, 2878-2889,  
707 10.1021/acs.est.0c06838, 2021.

708 Huang, L., Liu, T., and Grassian, V. H.: Radical-initiated formation of aromatic organosulfates  
709 and sulfonates in the aqueous phase, Environ. Sci. Technol., 54, 11857-11864,  
710 10.1021/acs.est.0c05644, 2020.

Formatted: Highlight

Formatted: Subscript, Highlight

Formatted: Highlight

Formatted: Highlight

Formatted: Highlight

Formatted: Highlight

Formatted: Highlight

Formatted: Highlight

711 Huang, R.-J., Yang, L., Shen, J., Yuan, W., Gong, Y., Ni, H., Duan, J., Yan, J., Huang, H., You,  
712 Q., and Li, Y. J.: Chromophoric fingerprinting of brown carbon from residential biomass burning,  
713 *Environ. Sci. Technol. Lett.*, 9, 102-111, 10.1021/acs.estlett.1c00837, 2021.

714 Huo, Y., Guo, Z., Li, Q., Wu, D., Ding, X., Liu, A., Huang, D., Qiu, G., Wu, M., Zhao, Z., Sun,  
715 H., Song, W., Li, X., Chen, Y., Wu, T., and Chen, J.: Chemical fingerprinting of HULIS in  
716 particulate matters emitted from residential coal and biomass combustion, *Environ. Sci. Technol.*,  
717 55, 3593-3603, 10.1021/acs.est.0c08518, 2021.

718 Jang, K. S., Choi, M., Park, M., Park, M. H., Kim, Y. H., Seo, J., Wang, Y., Hu, M., Bae, M. S.,  
719 and Park, K.: Assessment of PM<sub>2.5</sub>-bound nitrogen-containing organic compounds (NOCs) during  
720 winter at urban sites in China and Korea, *Environ. Pollut.*, 265, 114870,  
721 10.1016/j.envpol.2020.114870, 2020.

722 Jiang, B., Liang, Y., Xu, C., Zhang, J., Hu, M., and Shi, Q.: Polycyclic aromatic hydrocarbons  
723 (PAHs) in ambient aerosols from Beijing: characterization of low volatile PAHs by positive-ion  
724 atmospheric pressure photoionization (APPI) coupled with Fourier transform ion cyclotron  
725 resonance, *Environ. Sci. Technol.*, 48, 4716-4723, 10.1021/es405295p, 2014.

726 Jiang, H., Li, J., Chen, D., Tang, J., Cheng, Z., Mo, Y., Su, T., Tian, C., Jiang, B., Liao, Y., and  
727 Zhang, G.: Biomass burning organic aerosols significantly influence the light absorption properties  
728 of polarity-dependent organic compounds in the Pearl River Delta Region, China, *Environ. Int.*,  
729 144, 106079, 10.1016/j.envint.2020.106079, 2020.

730 Jiang, H., Li, J., Sun, R., Tian, C., Tang, J., Jiang, B., Liao, Y., Chen, C. E., and Zhang, G.:  
731 Molecular dynamics and light absorption properties of atmospheric dissolved organic matter,  
732 *Environ. Sci. Technol.*, 55, 10268-10279, 10.1021/acs.est.1c01770, 2021.

733 Koch, B. P., and Dittmar, T.: From mass to structure: an aromaticity index for high-resolution  
734 mass data of natural organic matter, *Rapid. Commun. Mass. Sp.*, 20, 926-932, 10.1002/rcm.2386,  
735 2006.

736 Kourtchev, I., Fuller, S., Aalto, J., Ruuskanen, T. M., McLeod, M. W., Maenhaut, W., Jones, R.,  
737 Kulmala, M., and Kalberer, M.: Molecular composition of boreal forest aerosol from Hyttiala,  
738 Finland, using ultrahigh resolution mass spectrometry, *Environ. Sci. Technol.*, 47, 4069-4079,  
739 10.1021/es3051636, 2013.

740 Kourtchev, I., O'Connor, I. P., Giorio, C., Fuller, S. J., Kristensen, K., Maenhaut, W., Wenger, J.  
741 C., Sodeau, J. R., Glasius, M., and Kalberer, M.: Effects of anthropogenic emissions on the

742 molecular composition of urban organic aerosols: An ultrahigh resolution mass spectrometry study,  
743 *Atmos. Environ.*, 89, 525-532, 10.1016/j.atmosenv.2014.02.051, 2014.

744 Kourtchev, I., Godoi, R. H. M., Connors, S., Levine, J. G., Archibald, A. T., Godoi, A. F. L.,  
745 Paralovo, S. L., Barbosa, C. G. G., Souza, R. A. F., Manzi, A. O., Seco, R., Sjostedt, S., Park, J.-  
746 H., Guenther, A., Kim, S., Smith, J., Martin, S. T., and Kalberer, M.: Molecular composition of  
747 organic aerosols in central Amazonia: an ultra-high-resolution mass spectrometry study, *Atmos.*  
748 *Chem. Phys.*, 16, 11899-11913, 10.5194/acp-16-11899-2016, 2016.

749 Kroll, J. H., Donahue, N. M., Jimenez, J. L., Kessler, S. H., Canagaratna, M. R., Wilson, K. R.,  
750 Altieri, K. E., Mazzoleni, L. R., Wozniak, A. S., Bluhm, H., Mysak, E. R., Smith, J. D., Kolb, C.  
751 E., and Worsnop, D. R.: Carbon oxidation state as a metric for describing the chemistry of  
752 atmospheric organic aerosol, *Nat. Chem.*, 3, 133-139, 10.1038/nchem.948, 2011.

753 Kuang, B. Y., Lin, P., Huang, X. H. H., and Yu, J. Z.: Sources of humic-like substances in the  
754 Pearl River Delta, China: positive matrix factorization analysis of PM<sub>2.5</sub> major components and  
755 source markers, *Atmos. Chem. Phys.*, 15, 1995-2008, 10.5194/acp-15-1995-2015, 2015.

756 Laskin, A., Smith, J. S., and Laskin, J.: Molecular characterization of nitrogen-containing organic  
757 compounds in biomass burning aerosols using high-resolution mass spectrometry, *Environ. Sci.*  
758 *Technol.*, 43, 3764-3771, 10.1021/es803456n, 2009.

759 Laskin, J., Laskin, A., and Nizkorodov, S. A.: Mass spectrometry analysis in atmospheric  
760 chemistry, *Anal. Chem.*, 90, 166-189, 10.1021/acs.analchem.7b04249, 2018.

761 Levin, I., and Kromer, B.: The tropospheric <sup>14</sup>CO<sub>2</sub> level in mid-latitudes of the northern  
762 hemisphere (1959–2003), *Radiocarbon*, 46, 1261-1272, 10.1017/s0033822200033130, 2004.

763 Levin, I., Kromer, B., and Hammer, S.: Atmospheric Δ<sup>14</sup>CO<sub>2</sub> trend in Western European  
764 background air from 2000 to 2012, *Tellus. B.*, 65, 10.3402/tellusb.v65i0.20092, 2013.

765 Li, X., Han, J., Hopke, P. K., Hu, J., Shu, Q., Chang, Q., and Ying, Q.: Quantifying primary and  
766 secondary humic-like substances in urban aerosol based on emission source characterization and  
767 a source-oriented air quality model, *Atmos. Chem. Phys.*, 19, 2327-2341, 10.5194/acp-19-2327-  
768 2019, 2019.

769 Li, X., Yu, F., Cao, J., Fu, P., Hua, X., Chen, Q., Li, J., Guan, D., Tripathee, L., Chen, Q., and  
770 Wang, Y.: Chromophoric dissolved organic carbon cycle and its molecular compositions and  
771 optical properties in precipitation in the Guanzhong basin, China, *Sci. Total. Environ.*, 814, 152775,  
772 10.1016/j.scitotenv.2021.152775, 2022.

773 Lin, P., Rincon, A. G., Kalberer, M., and Yu, J. Z.: Elemental composition of HULIS in the Pearl  
774 River Delta Region, China: results inferred from positive and negative electrospray high resolution  
775 mass spectrometric data, *Environ. Sci. Technol.*, 46, 7454-7462, 10.1021/es300285d, 2012a.

776 Lin, P., Yu, J. Z., Engling, G., and Kalberer, M.: Organosulfates in humic-like substance fraction  
777 isolated from aerosols at seven locations in East Asia: a study by ultra-high-resolution mass  
778 spectrometry, *Environ. Sci. Technol.*, 46, 13118-13127, 10.1021/es303570v, 2012b.

779 Lin, P., Aiona, P. K., Li, Y., Shiraiwa, M., Laskin, J., Nizkorodov, S. A., and Laskin, A.: Molecular  
780 characterization of brown carbon in biomass burning aerosol particles, *Environ. Sci. Technol.*, 50,  
781 11815-11824, 10.1021/acs.est.6b03024, 2016.

782 Lin, P., Bluvstein, N., Rudich, Y., Nizkorodov, S. A., Laskin, J., and Laskin, A.: Molecular  
783 chemistry of atmospheric brown carbon inferred from a nationwide biomass burning event,  
784 *Environ. Sci. Technol.*, 51, 11561-11570, 10.1021/acs.est.7b02276, 2017.

785 Lin, P., Fleming, L. T., Nizkorodov, S. A., Laskin, J., and Laskin, A.: Comprehensive molecular  
786 characterization of atmospheric brown carbon by high resolution mass spectrometry with  
787 electrospray and atmospheric pressure photoionization, *Anal. Chem.*, 90, 12493-12502,  
788 10.1021/acs.analchem.8b02177, 2018.

789 Liu, X., Zhang, Y.-L., Peng, Y., Xu, L., Zhu, C., Cao, F., Zhai, X., Haque, M. M., Yang, C., Chang,  
790 Y., Huang, T., Xu, Z., Bao, M., Zhang, W., Fan, M., and Lee, X.: Chemical and optical properties  
791 of carbonaceous aerosols in Nanjing, eastern China: regionally transported biomass burning  
792 contribution, *Atmos. Chem. Phys.*, 19, 11213-11233, 10.5194/acp-19-11213-2019, 2019.

793 Ma, L., Li, B., Liu, Y., Sun, X., Fu, D., Sun, S., Thapa, S., Geng, J., Qi, H., Zhang, A., and Tian,  
794 C.: Characterization, sources and risk assessment of PM<sub>2.5</sub>-bound polycyclic aromatic  
795 hydrocarbons (PAHs) and nitrated PAHs (NPAHs) in Harbin, a cold city in Northern China, *J.*  
796 *Clean. Prod.*, 264, 10.1016/j.jclepro.2020.121673, 2020.

797 Ma, Y., Cheng, Y., Qiu, X., Cao, G., Fang, Y., Wang, J., Zhu, T., Yu, J., and Hu, D.: Sources and  
798 oxidative potential of water-soluble humic-like substances (HULIS<sub>ws</sub>) in fine particulate matter  
799 (PM<sub>2.5</sub>) in Beijing, *Atmos. Chem. Phys.*, 18, 5607-5617, 10.5194/acp-18-5607-2018, 2018.

800 Mo, Y., Li, J., Jiang, B., Su, T., Geng, X., Liu, J., Jiang, H., Shen, C., Ding, P., Zhong, G., Cheng,  
801 Z., Liao, Y., Tian, C., Chen, Y., and Zhang, G.: Sources, compositions, and optical properties of  
802 humic-like substances in Beijing during the 2014 APEC summit: Results from dual carbon isotope

803 and Fourier-transform ion cyclotron resonance mass spectrometry analyses, *Environ. Pollut.*, 239,  
804 322-331, 10.1016/j.envpol.2018.04.041, 2018.

805 Mohr, C., Lopez-Hilfiker, F. D., Zotter, P., Prevot, A. S., Xu, L., Ng, N. L., Herndon, S. C.,  
806 Williams, L. R., Franklin, J. P., Zahniser, M. S., Worsnop, D. R., Knighton, W. B., Aiken, A. C.,  
807 Gorkowski, K. J., Dubey, M. K., Allan, J. D., and Thornton, J. A.: Contribution of nitrated phenols  
808 to wood burning brown carbon light absorption in Detling, United Kingdom during winter time,  
809 *Environ. Sci. Technol.*, 47, 6316-6324, 10.1021/es400683v, 2013.

810 Mutzel, A., Poulain, L., Berndt, T., Iinuma, Y., Rodigast, M., Boge, O., Richters, S., Spindler, G.,  
811 Sipila, M., Jokinen, T., Kulmala, M., and Herrmann, H.: Highly oxidized multifunctional organic  
812 compounds observed in tropospheric particles: a field and laboratory study, *Environ. Sci. Technol.*,  
813 49, 7754-7761, 10.1021/acs.est.5b00885, 2015.

814 Ning, C., Gao, Y., Zhang, H., Yu, H., Wang, L., Geng, N., Cao, R., and Chen, J.: Molecular  
815 characterization of dissolved organic matters in winter atmospheric fine particulate matters (PM<sub>2.5</sub>)  
816 from a coastal city of northeast China, *Sci. Total. Environ.*, 689, 312-321,  
817 10.1016/j.scitotenv.2019.06.418, 2019.

818 Ning, C., Gao, Y., Yu, H., Zhang, H., Geng, N., Cao, R., and Chen, J.: FT-ICR mass spectrometry  
819 for molecular characterization of water-insoluble organic compounds in winter atmospheric fine  
820 particulate matters, *J. Environ. Sci.*, 111, 51-60, 10.1016/j.jes.2020.12.017, 2022.

821 Noziere, B., Kalberer, M., Claeys, M., Allan, J., D'Anna, B., Decesari, S., Finessi, E., Glasius, M.,  
822 Grgic, I., Hamilton, J. F., Hoffmann, T., Iinuma, Y., Jaoui, M., Kahnt, A., Kampf, C. J., Kourtchev,  
823 I., Maenhaut, W., Marsden, N., Saarikoski, S., Schnelle-Kreis, J., Surratt, J. D., Szidat, S.,  
824 Szmigielski, R., and Wisthaler, A.: The molecular identification of organic compounds in the  
825 atmosphere: state of the art and challenges, *Chem. Rev.*, 115, 3919-3983, 10.1021/cr5003485,  
826 2015.

827 O'Brien, R. E., Laskin, A., Laskin, J., Rubitschun, C. L., Surratt, J. D., and Goldstein, A. H.:  
828 Molecular characterization of S- and N-containing organic constituents in ambient aerosols by  
829 negative ion mode high-resolution Nanospray desorption electrospray ionization mass  
830 spectrometry: CalNex 2010 field study, *J. Geophys. Res. -Atmos.*, 119, 10.1002/2014jd021955,  
831 2014.

832 Patriarca, C., Bergquist, J., Sjoberg, P. J. R., Tranvik, L., and Hawkes, J. A.: Online HPLC-ESI-  
833 HRMS method for the analysis and comparison of different dissolved organic matter samples,  
834 *Environ. Sci. Technol.*, 52, 2091-2099, 10.1021/acs.est.7b04508, 2018.

835 Pospisilova, V., Lopez-Hilfiker, F. D., Bell, D. M., Haddad, I. E., Mohr, C., Huang, W., Heikkinen,  
836 L., Xiao, M., Dommen, J., Prevot, A. S. H., Baltensperger, U., and Slowik, J. G.: On the fate of  
837 oxygenated organic molecules in atmospheric aerosol particles, *Sci. Adv.*, 6, 2020.

838 Qi, L., Zhang, Z., Wang, X., Deng, F., Zhao, J., and Liu, H.: Molecular characterization of  
839 atmospheric particulate organosulfates in a port environment using ultrahigh resolution mass  
840 spectrometry: Identification of traffic emissions, *J. Hazard. Mater.*, 419, 126431,  
841 10.1016/j.jhazmat.2021.126431, 2021.

842 Riva, M., Tomaz, S., Cui, T., Lin, Y.-H., Perraudin, E., Gold, A., Stone, E. A., Villenave, E., and  
843 Surratt, J. D.: Evidence for an unrecognized secondary anthropogenic source of organosulfates and  
844 sulfonates: gas-phase oxidation of polycyclic aromatic hydrocarbons in the presence of sulfate  
845 aerosol, *Environ. Sci. Technol.*, 49, 6654-6664, 10.1021/acs.est.5b00836, 2015.

846 Shen, H., Zhao, D., Pullinen, I., Kang, S., Vereecken, L., Fuchs, H., Acir, I. H., Tillmann, R.,  
847 Rohrer, F., Wildt, J., Kiendler-Scharr, A., Wahner, A., and Mentel, T. F.: Highly oxygenated  
848 organic nitrates formed from NO<sub>3</sub> radical-initiated oxidation of beta-Pinene, *Environ. Sci.*  
849 *Technol.*, 10.1021/acs.est.1c03978, 2021.

850 Siemens, K., Morales, A., He, Q., Li, C., Hettiyadura, A. P. S., Rudich, Y., and Laskin, A.:  
851 Molecular analysis of secondary brown carbon produced from the photooxidation of naphthalene,  
852 *Environ. Sci. Technol.*, 2022.

853 Song, J., Li, M., Jiang, B., Wei, S., Fan, X., and Peng, P.: Molecular characterization of water-  
854 soluble humic like substances in smoke particles emitted from combustion of biomass materials  
855 and coal using Ultrahigh-resolution electrospray ionization fourier transform ion cyclotron  
856 resonance mass spectrometry, *Environ. Sci. Technol.*, 52, 2575-2585, 10.1021/acs.est.7b06126,  
857 2018.

858 Song, J., Li, M., Fan, X., Zou, C., Zhu, M., Jiang, B., Yu, Z., Jia, W., Liao, Y., and Peng, P.:  
859 Molecular characterization of water- and methanol-soluble organic compounds emitted from  
860 residential coal combustion using Ultrahigh-resolution electrospray ionization fourier transform  
861 ion cyclotron resonance mass spectrometry, *Environ. Sci. Technol.*, 53, 13607-13617,  
862 10.1021/acs.est.9b04331, 2019.

863 Song, J., Li, M., Zou, C., Cao, T., Fan, X., Jiang, B., Yu, Z., Jia, W., and Peng, P.: Molecular  
864 characterization of nitrogen-containing compounds in humic-like substances emitted from  
865 biomass burning and coal combustion, *Environ. Sci. Technol.*, 56, 119-130,  
866 10.1021/acs.est.1c04451, 2022.

867 Sun, H., Li, X., Zhu, C., Huo, Y., Zhu, Z., Wei, Y., Yao, L., Xiao, H., and Chen, J.: Molecular  
868 composition and optical property of humic-like substances (HULIS) in winter-time PM<sub>2.5</sub> in the  
869 rural area of North China Plain, *Atmos. Environ.*, 252, 10.1016/j.atmosenv.2021.118316, 2021.

870 Surratt, J. D., Gómez-González, Y., Chan, A. W. H., Vermeylen, R., Shahgholi, M., Kleindienst,  
871 T. E., Edney, E. O., Offenberg, J. H., Lewandowski, M., Jaoui, M., Maenhaut, W., Claeys, M.,  
872 Flagan, R. C., and Seinfeld, J. H.: Organosulfate formation in biogenic secondary organic aerosol,  
873 *J. Phys. Chem. A* 112, 8345-8378, 10.1021/jp802310p, 2008.

874  
875 Tang, J., Li, J., Su, T., Han, Y., Mo, Y., Jiang, H., Cui, M., Jiang, B., Chen, Y., Tang, J., Song, J.,  
876 Peng, P. a., and Zhang, G.: Molecular compositions and optical properties of dissolved brown  
877 carbon in biomass burning, coal combustion, and vehicle emission aerosols illuminated by  
878 excitation–emission matrix spectroscopy and Fourier transform ion cyclotron resonance mass  
879 spectrometry analysis, *Atmos. Chem. Phys.*, 20, 2513-2532, 10.5194/acp-20-2513-2020, 2020.

880 Tao, S., Lu, X., Levac, N., Bateman, A. P., Nguyen, T. B., Bones, D. L., Nizkorodov, S. A., Laskin,  
881 J., Laskin, A., and Yang, X.: Molecular characterization of organosulfates in organic aerosols from  
882 Shanghai and Los Angeles urban areas by nanospray-desorption electrospray ionization high-  
883 resolution mass spectrometry, *Environ. Sci. Technol.*, 48, 10993-11001, 10.1021/es5024674, 2014.  
884 Tsui, W. G., and McNeill, V. F.: Modeling secondary organic aerosol production from  
885 photosensitized humic-like substances (HULIS), *Environ. Sci. Technol. Lett.*, 5, 255-259,  
886 10.1021/acs.estlett.8b00101, 2018.

887 Wang, J., Ge, X., Chen, Y., Shen, Y., Zhang, Q., Sun, Y., Xu, J., Ge, S., Yu, H., and Chen, M.:  
888 Highly time-resolved urban aerosol characteristics during springtime in Yangtze River Delta,  
889 China: insights from soot particle aerosol mass spectrometry, *Atmos. Chem. Phys.*, 16, 9109–9127,  
890 <https://doi.org/10.5194/acp-16-9109-2016>, 2016a.

891 Wang, J., Nie, W., Cheng, Y., Shen, Y., Chi, X., Wang, J., Huang, X., Xie, Y., Sun, P., Xu, Z., Qi,  
892 X., Su, H., and Ding, A.: Light absorption of brown carbon in eastern China based on 3-year multi-

Formatted: Highlight

Formatted: Highlight

Formatted: Highlight



893 wavelength aerosol optical property observations and an improved absorption Ångström exponent  
894 segregation method, *Atmos. Chem. Phys.*, 18, 9061-9074, 10.5194/acp-18-9061-2018, 2018a.  
895 Wang, J., Zhao, B., Wang, S., Yang, F., Xing, J., Morawska, L., Ding, A., Kulmala, M., Kerminen,  
896 V.-M., Kujansuu, J., Wang, Z., Ding, D., Zhang, X., Wang, H., Tian, M., Petäjä, T., Jiang, J., and  
897 Hao, J.: Particulate matter pollution over China and the effects of control policies, *Sci. Total*  
898 *Environ.*, 584–585, 426–447, <https://doi.org/10.1016/j.scitotenv.2017.01.027>, 2017a.  
899 Wang, K., Zhang, Y., Huang, R.-J., Cao, J., and Hoffmann, T.: UHPLC-Orbitrap mass  
900 spectrometric characterization of organic aerosol from a central European city (Mainz, Germany)  
901 and a Chinese megacity (Beijing), *Atmos. Environ.*, 189, 22-29, 10.1016/j.atmosenv.2018.06.036,  
902 2018a2018b.  
903 Wang, K., Zhang, Y., Huang, R. J., Wang, M., Ni, H., Kampf, C. J., Cheng, Y., Bilde, M., Glasius,  
904 M., and Hoffmann, T.: Molecular characterization and source identification of atmospheric  
905 particulate organosulfates using ultrahigh resolution mass spectrometry, *Environ. Sci. Technol.*,  
906 53, 6192-6202, 10.1021/acs.est.9b02628, 2019a.  
907 Wang, X., Hayeck, N., Brüggemann, M., Yao, L., Chen, H., Zhang, C., Emmelin, C., Chen, J.,  
908 George, C., and Wang, L.: Chemical characteristics of organic aerosols in Shanghai: a Study by  
909 Ultrahigh-performance liquid chromatography coupled with orbitrap mass spectrometry, *J.*  
910 *Geophys. Res. -Atmos.*, 122, 11,703-711,722, 10.1002/2017jd026930, 2017a2017b.  
911 Wang, X., Heald, C. L., Liu, J., Weber, R. J., Campuzano-Jost, P., Jimenez, J. L., Schwarz, J. P.,  
912 and Perring, A. E.: Exploring the observational constraints on the simulation of brown carbon,  
913 *Atmos. Chem. Phys.*, 18, 635-653, 10.5194/acp-18-635-2018, 2018b2018c.  
914 Wang, X. K., Rossignol, S., Ma, Y., Yao, L., Wang, M. Y., Chen, J. M., George, C., and Wang,  
915 L.: Molecular characterization of atmospheric particulate organosulfates in three megacities at the  
916 middle and lower reaches of the Yangtze River, *Atmos. Chem. Phys.*, 16, 2285-2298, 10.5194/acp-  
917 16-2285-2016, 2016b.  
918 Wang, Y., Hu, M., Lin, P., Guo, Q., Wu, Z., Li, M., Zeng, L., Song, Y., Zeng, L., Wu, Y., Guo, S.,  
919 Huang, X., and He, L.: Molecular characterization of nitrogen-containing organic compounds in  
920 humic-like substances emitted from straw residue burning, *Environ. Sci. Technol.*, 51, 5951-5961,  
921 10.1021/acs.est.7b00248, 2017b2017c.  
922 Wang, Y., Hu, M., Guo, S., Wang, Y., Zheng, J., Yang, Y., Zhu, W., Tang, R., Li, X., Liu, Y., Le  
923 Breton, M., Du, Z., Shang, D., Wu, Y., Wu, Z., Song, Y., Lou, S., Hallquist, M., and Yu, J.: The

Formatted: Highlight

Formatted: Highlight

Formatted: Highlight

Formatted: Highlight

Formatted: Highlight

Formatted: Highlight

Formatted: Highlight

924 secondary formation of organosulfates under interactions between biogenic emissions and  
925 anthropogenic pollutants in summer in Beijing, *Atmos. Chem. Phys.*, 18, 10693-10713,  
926 10.5194/acp-18-10693-2018, [2018e2018d](#).

Formatted: Highlight

927 Wang, Y., Hu, M., Lin, P., Tan, T., Li, M., Xu, N., Zheng, J., Du, Z., Qin, Y., Wu, Y., Lu, S., Song,  
928 Y., Wu, Z., Guo, S., Zeng, L., Huang, X., and He, L.: Enhancement in particulate organic nitrogen  
929 and light absorption of humic-like substances over Tibetan Plateau due to long-range transported  
930 biomass burning emissions, *Environ. Sci. Technol.*, 53, 14222-14232, 10.1021/acs.est.9b06152,  
931 2019b.

932 Wang, Y., Hu, M., Wang, Y.-C., Li, X., Fang, X., Tang, R., Lu, S., Wu, Y., Guo, S., Wu, Z.,  
933 Hallquist, M., and Yu, J. Z.: Comparative study of particulate organosulfates in contrasting  
934 atmospheric environments: field evidence for the significant influence of anthropogenic sulfate  
935 and NO<sub>x</sub>, *Environ. Sci. Technol. Lett.*, 7, 787-794, 10.1021/acs.estlett.0c00550, 2020.

936 Willoughby, A. S., Wozniak, A. S., and Hatcher, P. G.: A molecular-level approach for  
937 characterizing water-insoluble components of ambient organic aerosol particulates using  
938 ultrahigh-resolution mass spectrometry, *Atmos. Chem. Phys.*, 14, 10299-10314, 10.5194/acp-14-  
939 10299-2014, 2014.

940 Wozniak, A. S., Bauer, J. E., Sleighter, R. L., Dickhut, R. M., and Hatcher, P. G.: Technical note:  
941 Molecular characterization of aerosol-derived water soluble organic carbon using ultrahigh  
942 resolution electrospray ionization Fourier transform ion cyclotron resonance mass spectrometry,  
943 *Atmos. Chem. Phys.*, 8, 5099–5111, [www.atmos-chem-phys.net/8/5099/2008/](http://www.atmos-chem-phys.net/8/5099/2008/), 2008.

944 Wu, C., Yang, J., Fu, Q., Zhu, B., Ruan, T., and Jiang, G.: Molecular characterization of water-  
945 soluble organic compounds in PM<sub>2.5</sub> using ultrahigh resolution mass spectrometry, *Sci. Total.*  
946 *Environ.*, 668, 917-924, 10.1016/j.scitotenv.2019.03.031, 2019a.

947 Wu, G., Ram, K., Fu, P., Wang, W., Zhang, Y., Liu, X., Stone, E. A., Pradhan, B. B., Dangol, P.  
948 M., Panday, A. K., Wan, X., Bai, Z., Kang, S., Zhang, Q., and Cong, Z.: Water-soluble brown  
949 carbon in atmospheric aerosols from Godavari (Nepal), a regional representative of South Asia,  
950 *Environ. Sci. Technol.*, 53, 3471-3479, 10.1021/acs.est.9b00596, 2019b.

951 [Xu, B., Cheng, Z., Gustafsson, Ö., Kawamura, K., Jin, B., Zhu, S., Tang, T., Zhang, B., Li, J., and](#)  
952 [Zhang, G.: Compound-specific radiocarbon analysis of low molecular weight dicarboxylic acids](#)  
953 [in ambient aerosols using preparative gas chromatography: method development, \*Environ. Sci.\*](#)  
954 [Technol. Lett., 8, 135-141, 10.1021/acs.estlett.0c00887, 2021.](#)

Formatted: Font color: Auto, Highlight

955 Xie, M., Chen, X., Hays, M. D., Lewandowski, M., Offenberg, J., Kleindienst, T. E., and Holder,  
956 A. L.: Light absorption of secondary organic aerosol: composition and contribution of  
957 nitroaromatic compounds, *Environ. Sci. Technol.*, 51, 11607-11616, 10.1021/acs.est.7b03263,  
958 2017.

959 [Xie, X., Chen, Y., Nie, D., Liu, Y., Liu, Y., Lei, R., Zhao, X., Li, H., and Ge, X.: Light-absorbing  
960 and fluorescent properties of atmospheric brown carbon: A case study in Nanjing, China.  
961 \*Chemosphere\*, 251, 126350, 10.1016/j.chemosphere.2020.126350, 2020.](#)

Formatted: Highlight

962 Yang, Z., Tsona, N. T., Li, J., Wang, S., Xu, L., You, B., and Du, L.: Effects of NO<sub>x</sub> and SO<sub>2</sub> on  
963 the secondary organic aerosol formation from the photooxidation of 1,3,5-trimethylbenzene: A  
964 new source of organosulfates, *Environ. Pollut.*, 264, 114742, 10.1016/j.envpol.2020.114742, 2020.

965 Yang, Z., Tsona, N. T., George, C., and Du, L.: Nitrogen-containing compounds enhance Light  
966 absorption of aromatic-derived brown carbon, *Environ. Sci. Technol.*, 10.1021/acs.est.1c08794,  
967 2022.

968 [Zeng, Y., Ning, Y., Shen, Z., Zhang, L., Zhang, T., Lei, Y., Zhang, Q., Li, G., Xu, H., Ho, S. S.  
969 H., and Cao, J.: The roles of N, S, and O in molecular absorption features of brown carbon in PM<sub>2.5</sub>  
970 in a typical semi-arid megacity in Northwestern China, \*J. Geophys. Res: Atmospheres\*, 126,  
971 10.1029/2021jd034791, 2021.](#)

Formatted: Highlight

Formatted: Subscript, Highlight

Formatted: Highlight

972 Zhang, A., Wang, Y., Zhang, Y., Weber, R. J., Song, Y., Ke, Z., and Zou, Y.: Modeling the global  
973 radiative effect of brown carbon: a potentially larger heating source in the tropical free troposphere  
974 than black carbon, *Atmos. Chem. Phys.*, 20, 1901-1920, 10.5194/acp-20-1901-2020, 2020.

Formatted: Highlight

975 Zhang, R., Gen, M., Liang, Z., Li, Y. J., and Chan, C. K.: Photochemical reactions of glyoxal  
976 during particulate ammonium nitrate photolysis: brown carbon formation, enhanced glyoxal decay,  
977 and organic phase formation, *Environ. Sci. Technol.*, 56, 1605-1614, 10.1021/acs.est.1c07211,  
978 2022.

Formatted: Highlight

979 [Zhang, T., Shen, Z., Zhang, L., Tang, Z., Zhang, Q., Chen, Q., Lei, Y., Zeng, Y., Xu, H., and Cao,  
980 J.: PM<sub>2.5</sub> Humic-like substances over Xi'an, China: Optical properties, chemical functional group,  
981 and source identification, \*Atmos. Res.\*, 234, 10.1016/j.atmosres.2019.104784, 2020b.](#)

Formatted: Highlight

Formatted: Subscript, Highlight

Formatted: Highlight

982 [Zhang, T., Shen, Z., Zeng, Y., Cheng, C., Wang, D., Zhang, Q., Lei, Y., Zhang, Y., Sun, J., Xu,  
983 H., Ho, S. S. H., and Cao, J.: Light absorption properties and molecular profiles of HULIS in PM<sub>2.5</sub>  
984 emitted from biomass burning in traditional "Heated Kang" in Northwest China, \*Sci. Total  
985 Environ.\*, 776, 146014, 10.1016/j.scitotenv.2021.146014, 2021.](#)

Formatted: Highlight

Formatted: Subscript, Highlight

Formatted: Highlight

Formatted: Highlight

Formatted: Highlight

Formatted: Highlight

986 Zhang, T., Huang, S., Wang, D., Sun, J., Zhang, Q., Xu, H., Hang Ho, S. S., Cao, J., and Shen, Z.:  
987 Seasonal and diurnal variation of PM<sub>2.5</sub>HULIS over Xi'an in Northwest China: Optical properties,  
988 chemical functional group, and relationship with reactive oxygen species (ROS), *Atmos. Environ.*,  
989 268, 118782, <https://doi.org/10.1016/j.atmosenv.2021.118782>, 2022b.  
990 Zhang, T., Shen, Z., Huang, S., Lei, Y., Zeng, Y., Sun, J., Zhang, Q., Ho, S. S. H., Xu, H., and  
991 Cao, J.: Optical properties, molecular characterizations, and oxidative potentials of different  
992 polarity levels of water-soluble organic matters in winter PM<sub>2.5</sub> in six China's megacities, *Sci. Total*  
993 *Environ.*, 853, 158600, <https://doi.org/10.1016/j.scitotenv.2022.158600>, 2022c.  
994  
995 Zhang, Y., Forrister, H., Liu, J., Dibb, J., Anderson, B., Schwarz, J. P., Perring, A. E., Jimenez, J.  
996 L., Campuzano-Jost, P., Wang, Y., Nenes, A., and Weber, R. J.: Top-of-atmosphere radiative  
997 forcing affected by brown carbon in the upper troposphere, *Nat. Geosci.*, 10, 486-489,  
998 10.1038/NGEO2960, 2017.  
999 Zhao, M., Qiao, T., Li, Y., Tang, X., Xiu, G., and Yu, J. Z.: Temporal variations and source  
1000 apportionment of Hulis-C in PM<sub>2.5</sub> in urban Shanghai, *Sci. Total. Environ.*, 571, 18-26,  
1001 [10.1016/j.scitotenv.2016.07.127](https://doi.org/10.1016/j.scitotenv.2016.07.127), 2016.  
1002 Zhao, Y., Hallar, A. G., and Mazzoleni, L. R.: Atmospheric organic matter in clouds: exact masses  
1003 and molecular formula identification using ultrahigh-resolution FT-ICR mass spectrometry,  
1004 *Atmos. Chem. Phys.*, 13, 12343-12362, 10.5194/acp-13-12343-2013, 2013.  
1005 Zheng, G., He, K., Duan, F., Cheng, Y., and Ma, Y.: Measurement of humic-like substances in  
1006 aerosols: A review, *Environ. Pollut.*, 181, 301-314, 10.1016/j.envpol.2013.05.055, 2013.  
1007 Zheng, Y., Chen, Q., Cheng, X., Mohr, C., Cai, J., Huang, W., Shrivastava, M., Ye, P., Fu, P., Shi,  
1008 X., Ge, Y., Liao, K., Miao, R., Qiu, X., Koenig, T. K., and Chen, S.: Precursors and pathways  
1009 leading to enhanced secondary organic aerosol formation during severe haze episodes, *Environ.*  
1010 *Sci. Technol.*, 10.1021/acs.est.1c04255, 2021.

Formatted: Highlight

Formatted: Subscript, Highlight

Formatted: Highlight

Formatted: Highlight

Formatted: Highlight

Formatted: Subscript, Highlight

Formatted: Highlight

Formatted: Highlight

Formatted: Highlight

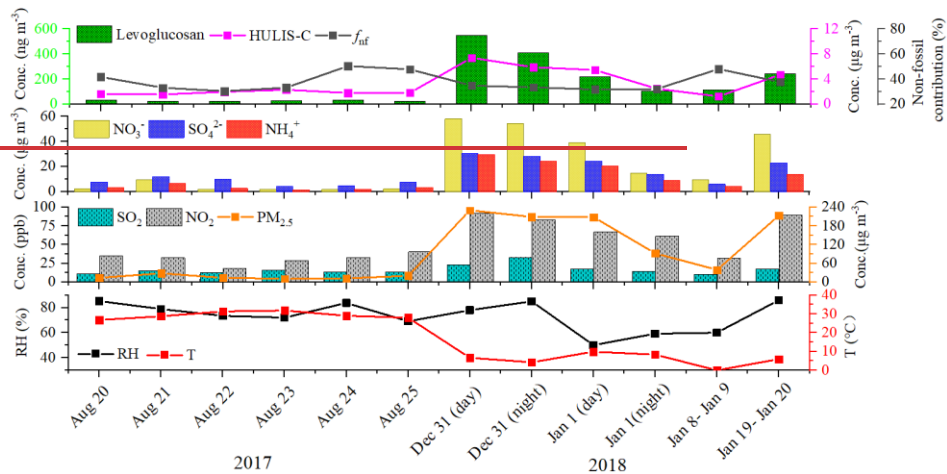
Formatted: Highlight

Formatted: Highlight

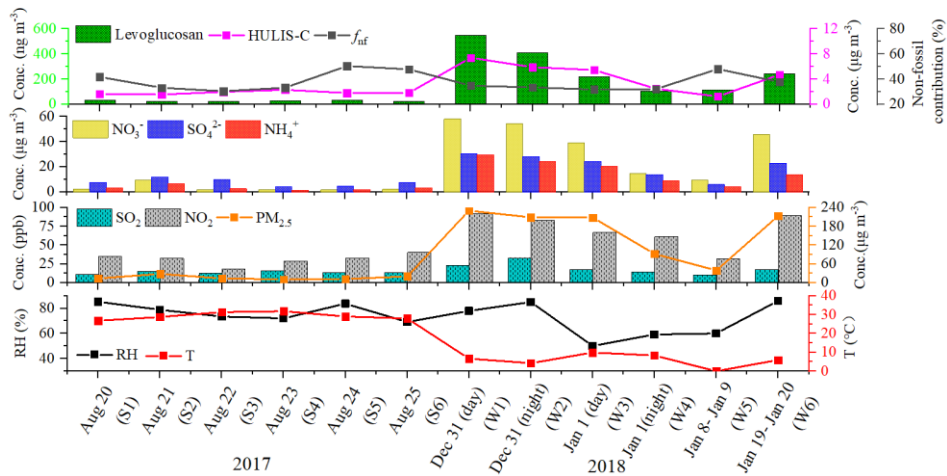
Formatted: Subscript, Highlight

Formatted: Highlight

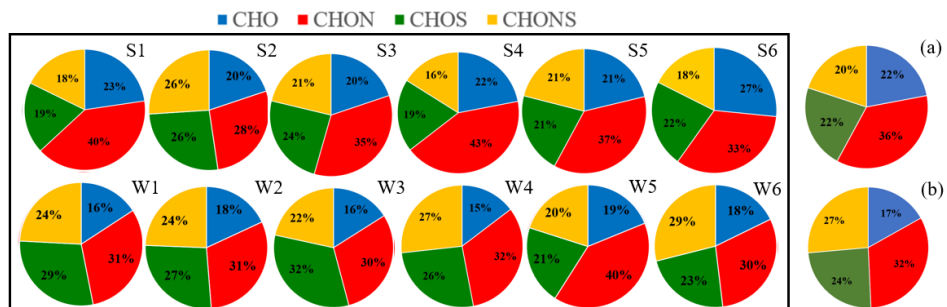
1011



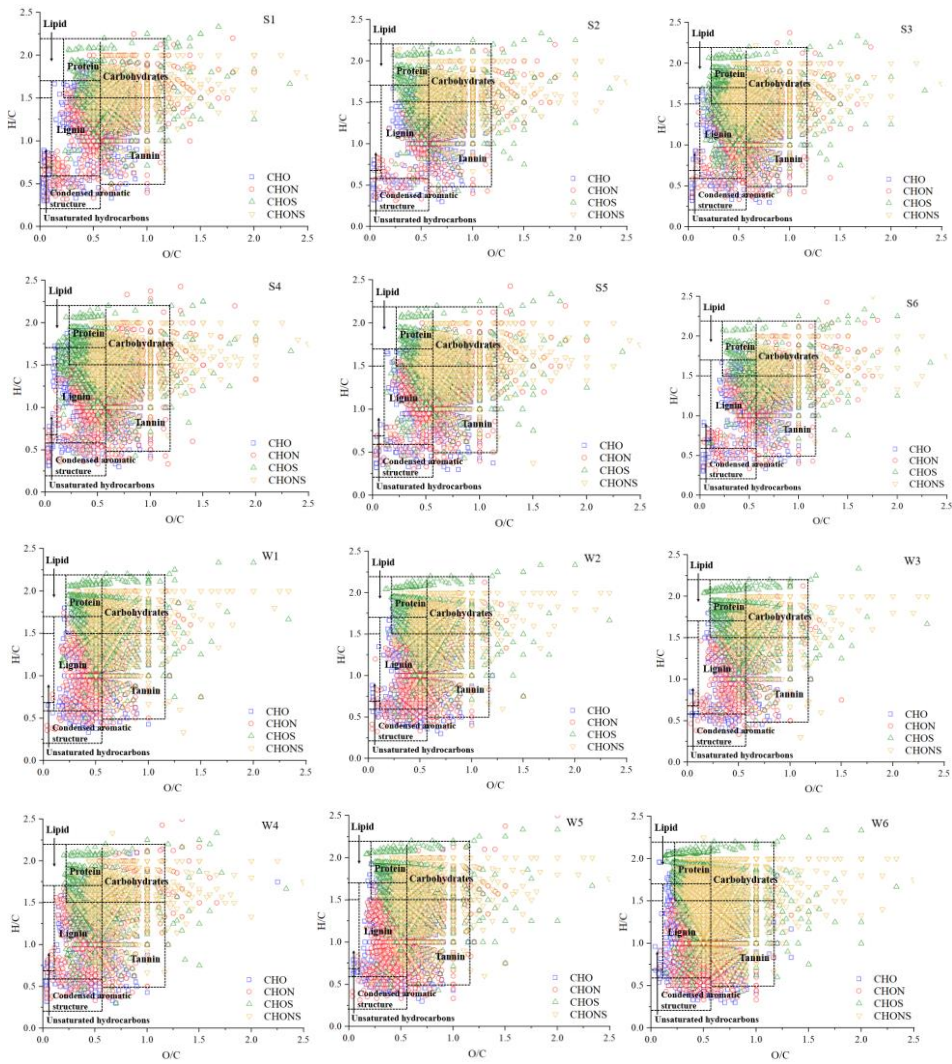
1012



1013 Figure 1. Time series of non-fossil contributions to HULIS-C, the mass concentrations of HULIS-  
 1014 C, Levoglucosan,  $\text{NO}_3^-$ ,  $\text{SO}_4^{2-}$ ,  $\text{NH}_4^+$ ,  $\text{SO}_2$ ,  $\text{NO}_2$ , and  $\text{PM}_{2.5}$ , relative humidity, and temperature  
 1015 during the study periods.



1016  
 1017 Figure 2. Pie graph of the number percentages of each elemental formula group for the 12 samples  
 1018 plotted in the box and the averaged number percentages of each elemental formula group for the  
 1019 summer samples (a) and winter samples (b).



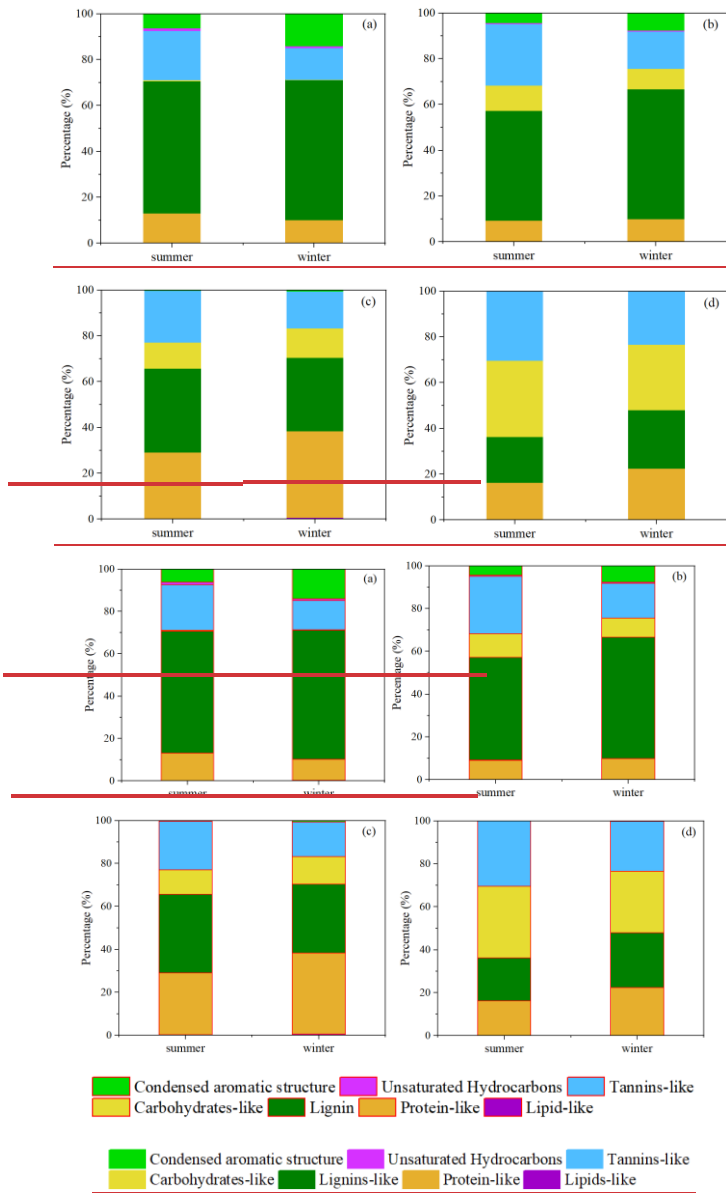
1020

1021

1022

1023

1024 Figure 3. Van Krevelen diagrams of the 12 samples.



1025

1026

1027

1028

1029

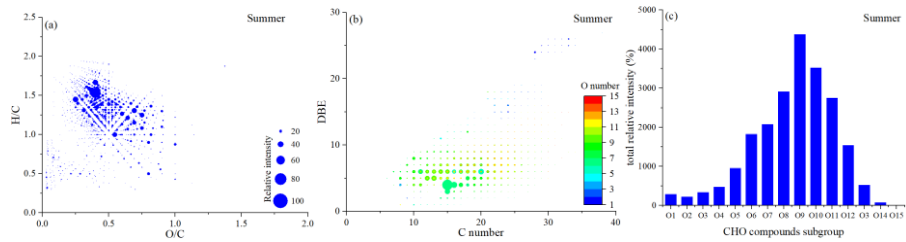
1030

1031 Figure 4. Contributions of seven categories in CHO (a), CHON (b), CHOS (c), and CHONS (d)

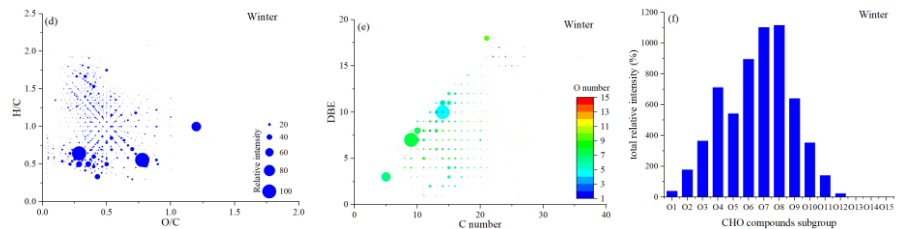
1032 compounds.



1033

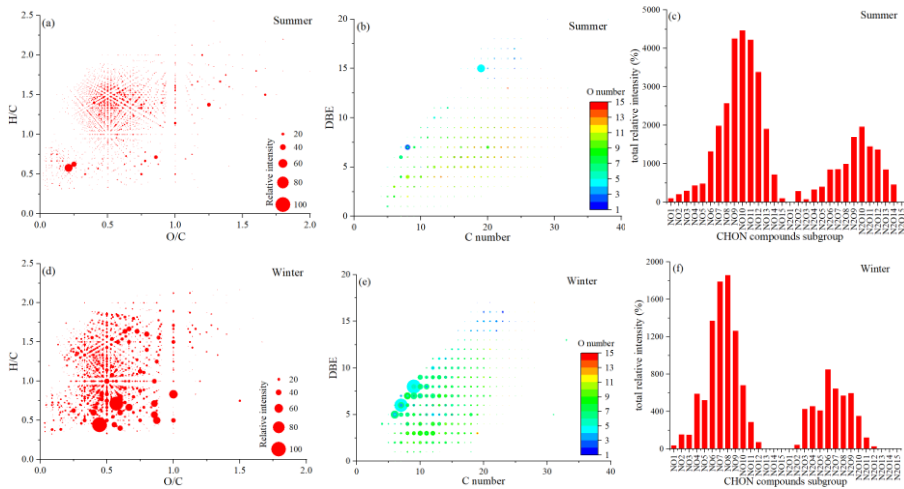


1034



1035 Figure 5. Van Krevelen diagram ((a) and (d)), plot of DBE values vs carbon atom numbers ((b)  
1036 and (e)), and the total relative intensity of each subgroup ((c) and (f)) for the CHO compounds in  
1037 summer and winter.

1038



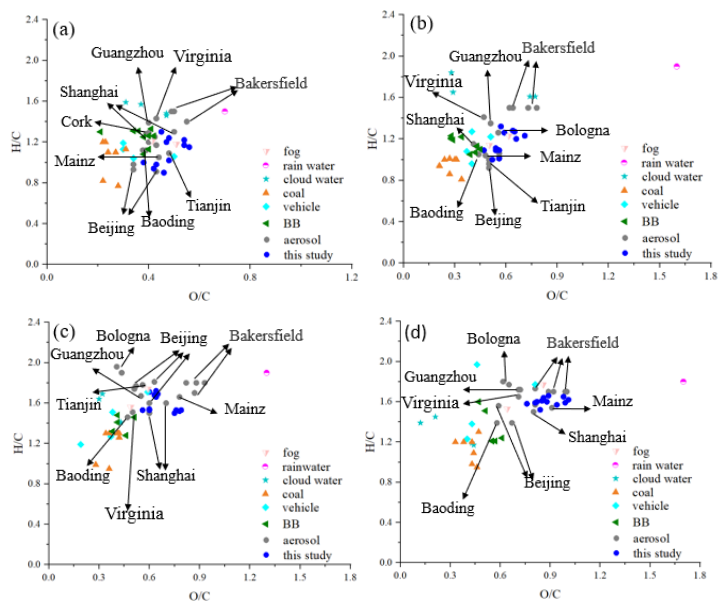
1039

1040 Figure 6. Van Krevelen diagram ((a) and (d)), plot of DBE values vs carbon atom numbers ((b)  
1041 and (e)), and the total relative intensity of each subgroup ((c) and (f)) for the CHON compounds  
1042 in summer and winter.





1054



1055

1056 Figure 9. Comparison of O/C and H/C ratios of water soluble organic compounds in different  
1057 atmospheric media in CHO (a), CHON (b), CHOS (c), and CHONS (d) compounds.